Molecular Therapy
Nucleic Acids
Original Article

Non-targeting control for MISSION shRNA library silences *SNRPD3* leading to cell death or permanent growth arrest

Maria Czarnek,[1] Katarzyna Sarad,[1,2] Agnieszka Karaś,[1,3] Jakub Kochan,[1] and Joanna Bereta[1]

[1]Department of Cell Biochemistry, Faculty of Biochemistry, Biophysics and Biotechnology, Jagiellonian University in Kraków, Gronostajowa 7, 30-387 Kraków, Poland

In parallel with the expansion of RNA interference (RNAi) techniques, accumulating evidence indicates that RNAi analyses might be seriously biased due to the off-target effects of gene-specific short hairpin RNAs (shRNAs). Our findings indicated that off-target effects of non-targeting shRNA comprise another source of misinterpreted shRNA-based data. We found that SHC016, which is one of two non-targeting shRNA controls for the MISSION (commercialized TRC) library, exerts deleterious effects that lead to elimination of the shRNA-coding cassette from the genomes of cultured murine and human cells. Here, we used a lentiviral vector with inducible SHC016 expression to confirm that this shRNA induces apoptosis in murine cells and senescence or mitotic catastrophe depending on the p53 status in human tumor cells. We identified the core spliceosomal protein, small nuclear ribonucleoprotein Sm D3 (SNRPD3), as a major SHC016 target in several cell lines and confirmed that CRISPRi knockdown of *SNRPD3* mimics the effects of SHC016 expression in A549 and U251 cells. The overexpression of SNRPD3 rescued U251 cells from SHC016-induced mitotic catastrophe. Our findings disqualified non-targeting SHC016 shRNA and added a new premise to the discussion about the sources of uncertainty in RNAi results.

INTRODUCTION

Gene functions can be determined by a loss-of-function approach using RNA interference (RNAi). The technique is based on the natural mechanisms of post-transcriptional gene silencing by short RNA species such as microRNA (miRNA) derived from endogenous precursors (pre-miRNAs) and small interfering RNA (siRNA) derived from exogenous long double-stranded (ds)RNA of viral origin.[1]

Primary miRNAs (pri-miRNAs) are processed in the nuclei of mammalian cells by the microprocessor complex to produce hairpin pre-miRNAs, which are further processed by the cytosolic endonuclease Dicer to miRNA duplexes with two nucleotide overhangs at the 3′ end of each RNA strand. Argonaute protein is loaded with one strand of the miRNA duplex to create an RNA-induced silencing complex (RISC), which interacts with a target mRNA leading to inhibition of its translation and/or degradation.[2]

miRNA-like siRNA duplexes that did not require endonucleolytic processing were initially designed and transfected into cells to silence genes of interest. However, inefficient transfection of many cell lines as well as the transience of siRNA activity have led to the development of short hairpin RNA (shRNA) expression vectors including retroviral and lentiviral vectors.[3] An expression cassette coding for a given shRNA is stably integrated into the DNA of transduced cells, and the transcribed shRNA, which mimics pre-miRNA, is processed by Dicer to an siRNA duplex.[4]

The need for unified research tools has triggered the development of shRNA libraries of sequences that silence individual genes in the same shRNA backbone. Engineered shRNA libraries have facilitated the development of high-throughput methods using arrayed or pooled RNAi screens to identify proteins involved in different cellular processes or novel specific therapeutic targets.[5–8]

A popular lentiviral TRC shRNA library has been developed by the RNAi Consortium at the Broad Institute and marketed by Merck (Darmstadt, Germany; previously Sigma-Aldrich, St. Louis, MO, USA) under the trade name MISSION. The library contains shRNAs targeting $\sim 15 \times 10^3$ human and $\sim 15 \times 10^3$ mouse transcripts, each of which is covered by an average of five shRNAs. The library was generated using the pLKO.1 backbone containing the puromycin-resistance gene and shRNA sequences flanked by Pol III-recognized elements: the human U6 promoter and the T-stretch termination signal.[6]

Received 20 December 2020; accepted 3 September 2021;
https://doi.org/10.1016/j.omtn.2021.09.004.

[2]Present address: Department of Medical Biotechnology, Faculty of Biochemistry, Biophysics and Biotechnology, Jagiellonian University in Kraków, Gronostajowa 7, 30-387 Kraków, Poland

[3]Present address: Jagiellonian Centre for Experimental Therapeutics (JCET), Jagiellonian University in Kraków, Bobrzyńskiego 14, 30-348 Kraków, Poland

Correspondence: Maria Czarnek, Department of Cell Biochemistry, Faculty of Biochemistry, Biophysics and Biotechnology, Jagiellonian University in Kraków, Gronostajowa 7, 30-387 Kraków, Poland.
E-mail: maria.czarnek@uj.edu.pl
Correspondence: Joanna Bereta, Department of Cell Biochemistry, Faculty of Biochemistry, Biophysics and Biotechnology, Jagiellonian University in Kraków, Gronostajowa 7, 30-387 Kraków, Poland.
E-mail: joanna.bereta@uj.edu.pl

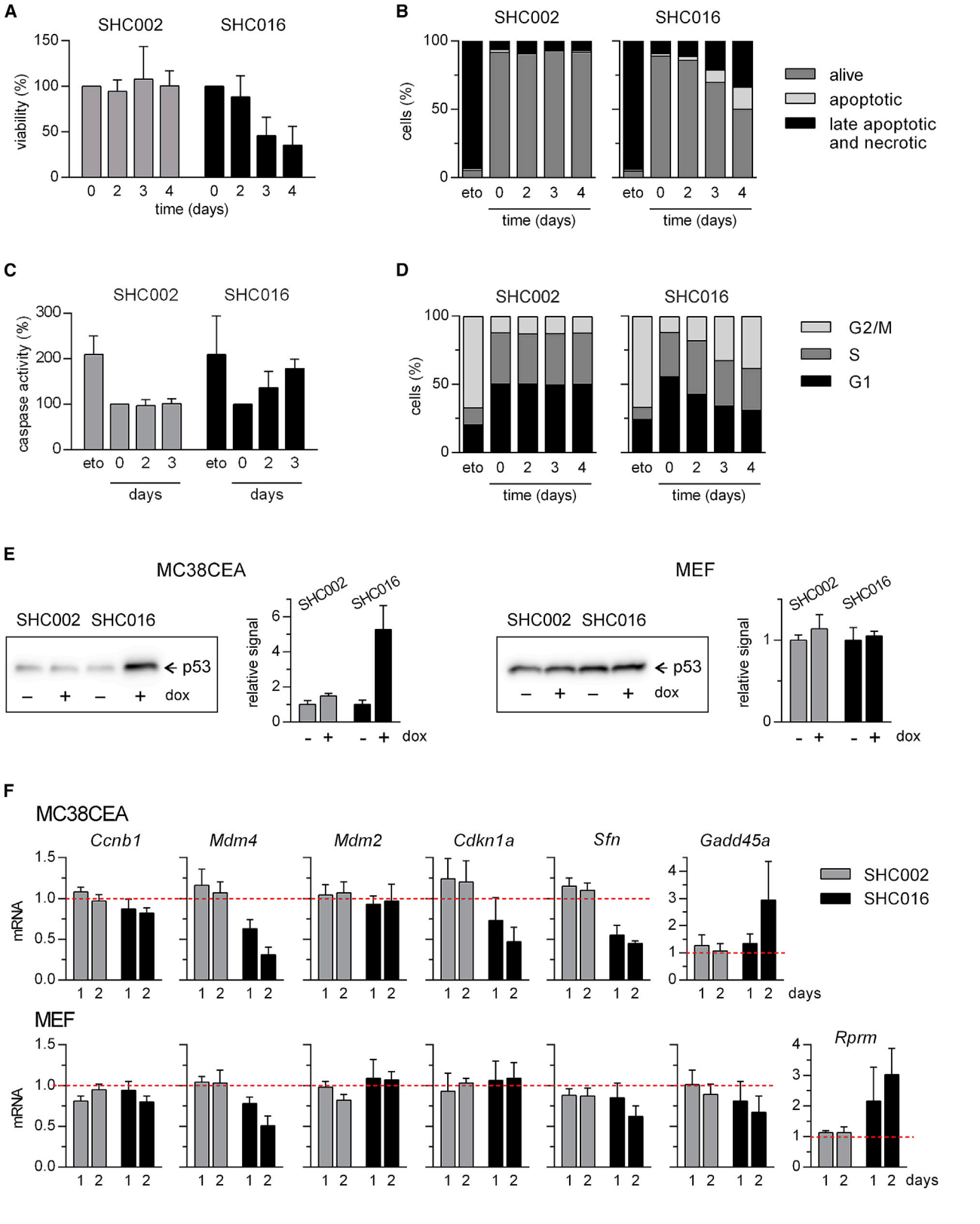

(legend on next page)

All experiments involving RNAi, including high-throughput screening and analyses of individual transcripts, require appropriate controls. An empty vector control does not contain any shRNA sequences and allows evaluation of the effects of transduction and of lentiviral vector elements (other than shRNA) on cells. A non-targeting shRNA control contains an shRNA-coding sequence that does not target any gene of a studied species. Cells transduced with a control lentiviral vector produce shRNAs that influence miRNA processing machinery and possibly other cellular processes according to non-specific effects triggered by gene-targeting shRNAs. This control should be used as a reference for all experimental results.

The MISSION library provides two non-targeting shRNA controls. One (SHC002) does not target mammalian transcripts, but it does target the turboGFP transcript and is therefore not recommended for cells expressing turboGFP. Supplier information states that the other non-targeting shRNA control (SHC016) does not target any transcript in any species according to bioinformatic data.[9]

We applied the SHC016 as a control in our studies and found that it had detrimental effects on transduced cells. We ruled out the possibility that the high rate of cell death was due to the puromycin effect on the cells that remained non-transduced. We accomplished this by generating vectors with the tetracycline/doxycycline-inducible expression of either SHC002 or SHC016, which enabled us to separate the processes of transduction/selection and shRNA expression. We then confirmed that SHC016 shRNA was cytotoxic using the vectors, Tet-on-SHC002 and Tet-on-SHC016. We also found that SHC016 induces different death pathways in murine and human cells and elucidated the mechanism of its action.

RESULTS

We considered that the MISSION non-targeting control shRNA, SHC016, is deleterious to transduced cells due to unusually high mortality of the cells after transduction. We therefore compared the effects the non-targeting shRNAs, SHC002 and SHC016, on MC38CEA cells transduced with the same amounts of either Tet-on-SHC002 or Tet-on-SHC016; then we used puromycin to select cells with incorporated transgenes. The cells were then cultured for 5 days with the expression of the non-targeting shRNAs switched on for the last 4, 3, or 2 days. Unlike SHC002, SHC016 significantly impacted transduced MC38CEA. The viability of the cells was measured using the colorimetric thiazolyl blue tetrazolium bromide (MTT) assay, in which MTT is reduced by metabolically active cells to purple formazan. The viability of MC38CEA cells decreased to ~30% on day 4 after inducing SHC016 expression (Figure 1A). The increased exposure of phosphatidylserine on the external leaflet of the plasma membrane detected by annexin V binding (Figures 1B and S1A) and the enhanced activity of the executioner caspase-3 and -7 (Figure 1C) indicated that the expression of SHC016 induced apoptosis in MC38CEA cells. This process was accompanied by an increase in the number of cells in the G2/M and a decrease in the number of cells in the G1 phase of the cell cycle, indicating cell-cycle arrest at the G2/M phase (Figures 1D and S1B).

The timing of the appearance and the magnitude of SHC016-mediated effects on murine embryonic fibroblast (MEF) viability and apoptosis resembled those for MC38CEA (Figure S2). However, unlike MC38CEA, the impact of SHC016 on the cell cycle of MEFs was weak and detectable only on day 4 of its expression but was nevertheless similar to MC38CEA in that the number of cells in the G2/M phase increased. Expression of shRNA can trigger an innate immune response, the interferon response that may result in cell death. We excluded the interferon response as the cause of SHC016-mediated effects because expression of the interferon-inducible genes *Oas1b*, *Ifit1*, and *Pkr* was not increased (Figure S3).

Because p53 accumulation is believed to be the major trigger of G2/M arrest, we analyzed the influences of SHC002 and SHC016 on p53 protein levels and the expression of p53 target genes including *Mdm2*, the apoptosis inducers *Bbc3* (also known as *Puma*) and *Pmaip1* (*Noxa*), as well as those involved in inhibition of G2/M transition such as *Cdkn1a* (coding for p21), *Gadd45a*, *Sfn* (stratifin; 14-3-3σ), and *Rprm* (reprimo) in MC38CEA cells and MEFs.[10,11] We also analyzed *Ccnb1*, which encodes mitotic cyclin (cyclin B1), and *Mdm4*, the product of which, apart from MDM2, binds p53 and inhibits its transcriptional activity.[12]

The expression of SHC016 resulted in substantially increased p53 levels in MC38CEA cells, indicating that SHC016 induced cellular stress (Figure 1E). Levels of p53 were high in all MEF cell lines regardless of the status of SHC002 or SHC016 expression (Figure 1E), which most likely reflected the activity of SV40 large T antigen (LT) that was used to immortalize MEF cells.[10] A typical p53 response was not switched on in either MC38CEA or MEF; levels of p53 target genes were mostly unaffected (*Bbc3*, *Pmaip1*; data not shown) or reduced

Figure 1. Expression of SHC016 in MC38CEA results in apoptosis and cell-cycle arrest at the G2/M phase

The expression of non-targeting shRNA SHC002 or SHC016 was induced by doxycycline (dox; 100 ng/mL) for the last 4, 3, or 2 days of the 5-day culture. (A) Cell viability assessed by MTT assay. Absorbance values of the cells without induced transgene expression were taken as 100%. (B) Analysis of death via apoptosis assessed by annexin V/PI staining and flow cytometry analysis; alive cells, annexin V^-/PI^-; apoptotic, annexin V^+/PI^-; and late apoptotic and necrotic, annexin V^+/PI^+ and annexin V^-/PI^+ (the latter usually did not exceed 3% of the cells expressing either shRNA). (C) Activity of caspase-3 and -7 measured via chemiluminescence assay. Chemiluminescence values of the cells without induced transgene expression were taken as 100%. (D) Flow cytometry analysis of the cell cycle. (B–D) The cells treated for the last 2 days of the experiment with etoposide (eto; 2 μM) were used as a positive control. (E) Western blot (WB) analysis of p53 levels in MC38CEA and MEF cells incubated for 48 h with or without dox. Luminescent signals were collected for approximately 3 min (MC38CEA) or 10 s (MEF). Representative images and quantifications of WB signals of three independent experiments are shown. Whole WB and Ponceau S-stained membranes are given in Figure S4. (F) qRT-PCR analysis of mRNA levels of p53 target genes in MC38CEA and MEF cells incubated for 1 or 2 days with or without dox. The relative levels of the transcripts in uninduced cells were taken as 1. (A–F) Data are shown as mean values (MVs) from 3 independent experiments. Error bars represent standard deviation (SD).

(*Cdkn1a* in MC38CEA and *Sfn* in both lines). The expression of LT might block the p53 response in MEFs.[13] Two mutations in *Tp53* have been identified in MC38 cells,[14] but their effect on p53 activity has not been studied. Our results suggested that they translate into deficient p53 transcriptional activity. This notion was also supported by the lack of substantial cytotoxicity of nutlin-3a, an inhibitor of MDM2-p53 interaction, toward MC38CEA cells (Figure S5).

Changes in the expression of genes related to cell-cycle control were found in MC38CEA cells and MEFs with induced expression of SHC016, but not SHC002, and the profiles of changes only partially overlapped between the cell lines (Figure 1F). The expression of *Mdm4* and *Sfn* was decreased, and that of *Ccnb1* was decreased to a small extent in both cell lines. The expression of *Gadd45a* was augmented only in MC38CEA cells. Levels of *Rprm*, which is undetectable in MC38CEA, were upregulated in MEFs expressing SHC016. The expression of both *Gadd45a* and *Rprm* might be upregulated by other transcription factors in addition to p53.[15,16] GADD45A is believed to affect cell-cycle progression via interactions with various molecules, such as PCNA, CDK1, and p21, and *Rprm* inhibits formation of the active cyclin B-CDK1 complex. Consequently, the expression of SHC016 induced distinct changes in the expression of genes related to cell-cycle control in the two mouse cell lines. Although these changes might affect the G2/M transition in MC38CEA and MEF cells, they did not imply the mechanism of SHC016 action.

We further analyzed the effects of the non-targeting sequences SHC002 and SHC016 on the human tumor cells A549, U251, HeLa, PC3, and MCF7 to determine whether the deleterious effects of SHC016 are limited to cells of murine origin or involve human cells. In contrast to SHC002, SHC016 potently impacted the viability of all cell lines (Figures 2A and S6).

We excluded the possibility that the negative effects of SHC016 were a matter of high transgene levels because qPCR analysis indicated that the levels of a pLKO cassette encoding SHC016 were comparable to or lower than those encoding SHC002 in all analyzed cell lines (Figure S7). The interferon response also did not occur in either A549 or U251 cells (Figure S8).

Unlike murine cells, apoptosis, evaluated using annexin V/propidium iodide (PI), did not seem to play a primary role in SHC016-mediated effects in human cells (data not shown). Cell-cycle analysis did not yield conclusive results. Therefore, we investigated whether the SHC016 sequence affects the proliferation or survival of human cells by simultaneously analyzing proliferation and viability after inducing non-targeting shRNAs expression; incorporation of bromodeoxyuridine (BrdU) indicated ongoing DNA synthesis associated with proliferation, and staining of dead cells indicated loss of viability (Figure 2B). The induction of SHC016 expression almost completely inhibited the incorporation of BrdU in A549 cells. The ratios (%) of U251, PC3, and HeLa cells that ceased to synthesize DNA did not increase or increased only slightly, whereas BrdU incorporation declined but to a lesser degree in MCF7 than in A549 cells. The type of response correlated with the p53 status of the cell lines. Only A549 cells express fully active p53, and the induction of SHC016 expression resulted in its accumulation in these cells (Figure 3A). Both U251 and PC3 express only mutated variants of p53, which cannot activate p53 target gene transcription, and wild-type (WT) *TP53* is transcribed in HeLa and MCF7 cell lines, but the activity of p53 protein is reduced.[11] The papilloma virus protease E6 degrades p53 in HeLa cells, and *MDM4* amplification impairs p53 functions in MCF7 cells.[11] Accordingly, SHC016 induced an increase in p53 levels in HeLa and MCF7 cells, although to a lesser extent than in A549 cells (Figure S9). However, growth arrest was irreversible independently of p53 status in cells with induced SHC016 expression; the results of colony formation assays showed that A549, U251, and HeLa cells lost the capacity to produce colonies (Figure 2C).

We speculated that SHC016 exerts deleterious effects via different mechanisms, one of which involved the activation of p53 in A549 cells. We then confirmed this notion and further elucidated the possible mechanism of SHC016-induced effects in A549 cells as follows. We used qRT-PCR to analyze potential changes in the expression of genes (1) activated by p53, including those encoding cell-cycle inhibitors and mediators of apoptosis (*CDKN1A*, *MDM2*, *BBC3*, *PMAIP1*, *GADD45A*, and *SFN*); (2) encoding central players in cell-cycle progression including *CDK2*, *CDK1*, *CCNB1*, *AURKA*, and *PLK1*, components of chromosomal passenger complex (*AURKB*, *BIRC5*, and *CDCA8*); and (3) encoding proteins of cell-cycle checkpoints (*CHEK1*, *CHEK2*, *BUB1*, *BUB1B*, *BUB3*, and *MAD2L1*). Switching on SHC016 but not SHC002 expression resulted in stimulation of the p53-regulated genes *CDKN1A*, *MDM2*, and *BBC3*, 24 h after adding doxycycline to the culture medium. This effect was further enhanced after 48 h (Figure 3B). The most stimulated gene was *CDKN1A*, which encodes p21, a universal inhibitor of cyclin-dependent kinases, and activates formation of the DREAM complex, which acts as a transcriptional repressor of genes involved in cell-cycle progression, including all genes in groups (2) and (3) above.[12] This explains the diminished levels of most of analyzed transcripts 48 h after inducing SHC016 expression (Figure S10) and halting A549 proliferation.

Analysis of *CDKN1A* expression in all studied cell lines revealed the absence of p53 transcriptional activity in U251, PC3, and MCF7 cells and slight activity in HeLa cells (Figure S11).

The expression of three potential p53 targets did not increase but rather decreased in A549 cells in response to SHC016: *PMAIP1*, *GADD45A*, and *SFN* (Figure 3B). These genes might be regulated by other mechanisms. Expression of the *Sfn* (mouse ortholog of *SFN*) was diminished in both murine cell lines expressing SHC016, and that of *Gadd45a* was diminished in MEF. Thus, we speculated that expression of SHC016 might impact the regulation of these transcript levels.

In addition to growth arrest, p21 might trigger a cellular senescence program,[13] in which cells permanently cease proliferation and have

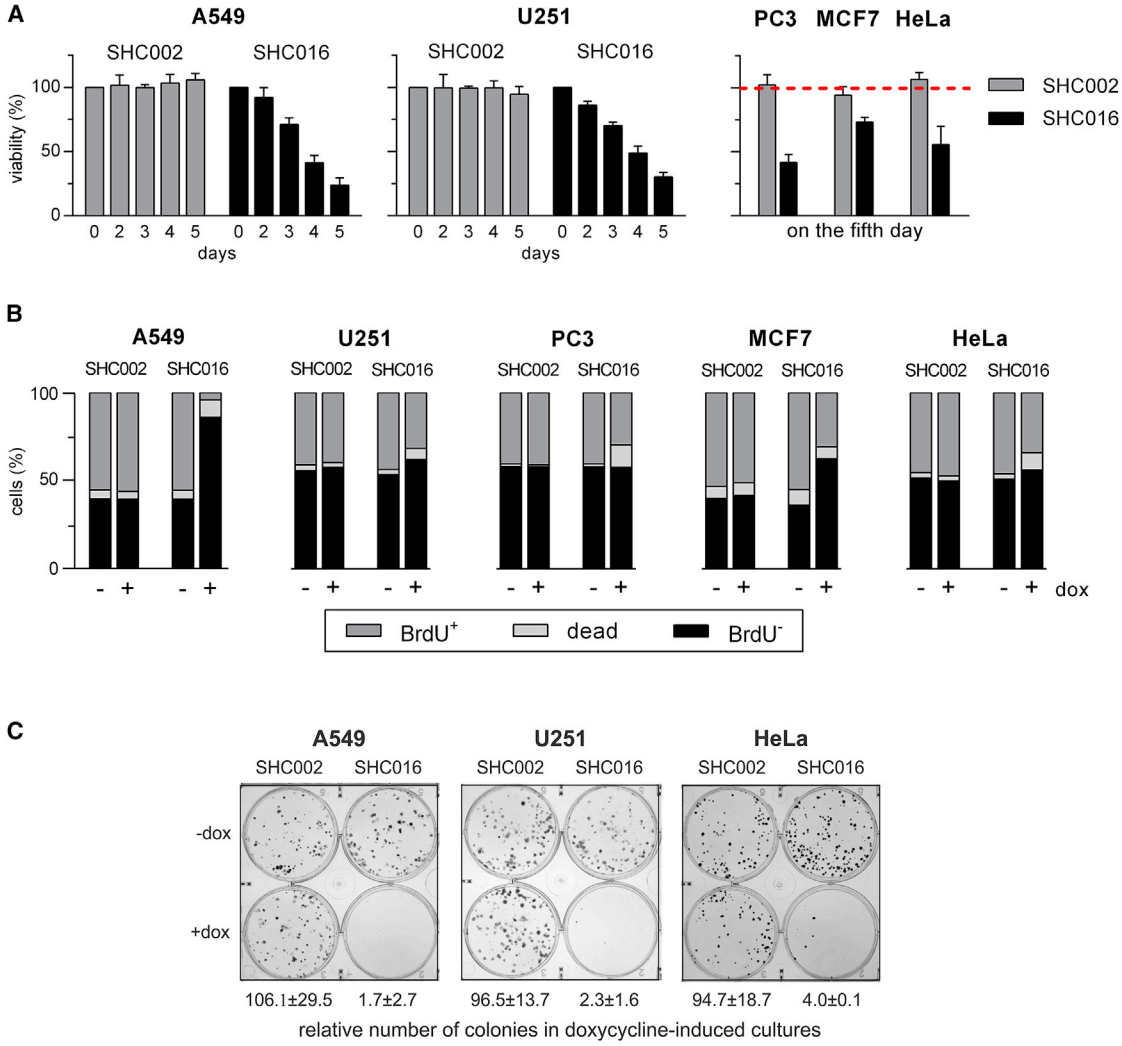

Figure 2. Expression of SHC016 in human cell lines results in inhibition of cell proliferation and/or viability

(A) Cell viability assessed by MTT assay. The expression of non-targeting shRNA SHC002 or SHC016 was induced by dox (100 ng/mL) for the last 5, 4, 3, or 2 days of the 6-day culture. The measurements taken each day (A549, U251) or on the 5th day of dox treatment (PC3, MCF7, HeLa) are shown. Full data for PC3, MCF7, and HeLa are available in Figure S6. Absorbance values of the cells without induction of shRNA expression were taken as 100%. (B) DNA synthesis and cell viability assessed via double BrdU/eFluor 520 viability staining were performed 3 (A549) or 5 (U251, PC3, MCF7, HeLa) days after inducing SHC002 or SHC016 expression. BrdU was added to the medium for the last 6 h of culture. The difference of the time schedule was dictated by shorter time needed to manifest cytostatic/cytotoxic effects of SHC016 in A549 and substantially shorter doubling time of A549 than of other cell lines (Table S1); dead, all eFluor 520$^+$ cells; BrdU$^+$, eFluor 520$^-$/BrdU$^+$ cells; and BrdU$^-$, eFluor 520$^-$/BrdU$^-$ cells. (A and B) Data are shown as MV from 3 independent experiments. (A) Error bars represent SD. (C) Analysis of clonal growth capacity of A549, U251, and HeLa cells by colony formation assay. Pictures of culture plates with stained clones were taken 7–10 days after plating the cells. Expression of SHC002 or SHC016 was induced with dox, 24 h after seeding the cells. The number of colonies in the corresponding, uninduced cultures was taken as 100%. Data are shown as MV ± SD from 3 (U251 and HeLa) or 4 (A549) independent experiments.

significantly altered morphology but remain metabolically active.[14–16] The key senescence marker, senescence-associated β-galactosidase (SA-β-gal), was active in 59.5% of A549 cells with induced SHC016 expression. In contrast, the ratios of SA-β-gal-positive cells among A549 cells without SHC016 induction or transduced with Tet-on-SHC002 were negligible (<1%) (Figure 3C). Enlarged and flattened areas of cells and irregular shapes are also characteristic of senescence (Figure 3C). The expression of SA-β-gal in PC3, HeLa, and U251 remained low despite SHC016 induction, whereas MCF7 cells expressed high levels of SA-β-gal independently of transduction with Tet-on vectors and doxycycline induction (data not shown).

SHC016 exerted harmful effects via different mechanisms in *TP53* mutant U251 and PC3 cells. Images of U251 and PC3 cells expressing SHC016 show hallmarks of mitotic catastrophe (MC) (Figures 4A and S12A–S12D). MC is a mechanism that senses aberrant mitosis

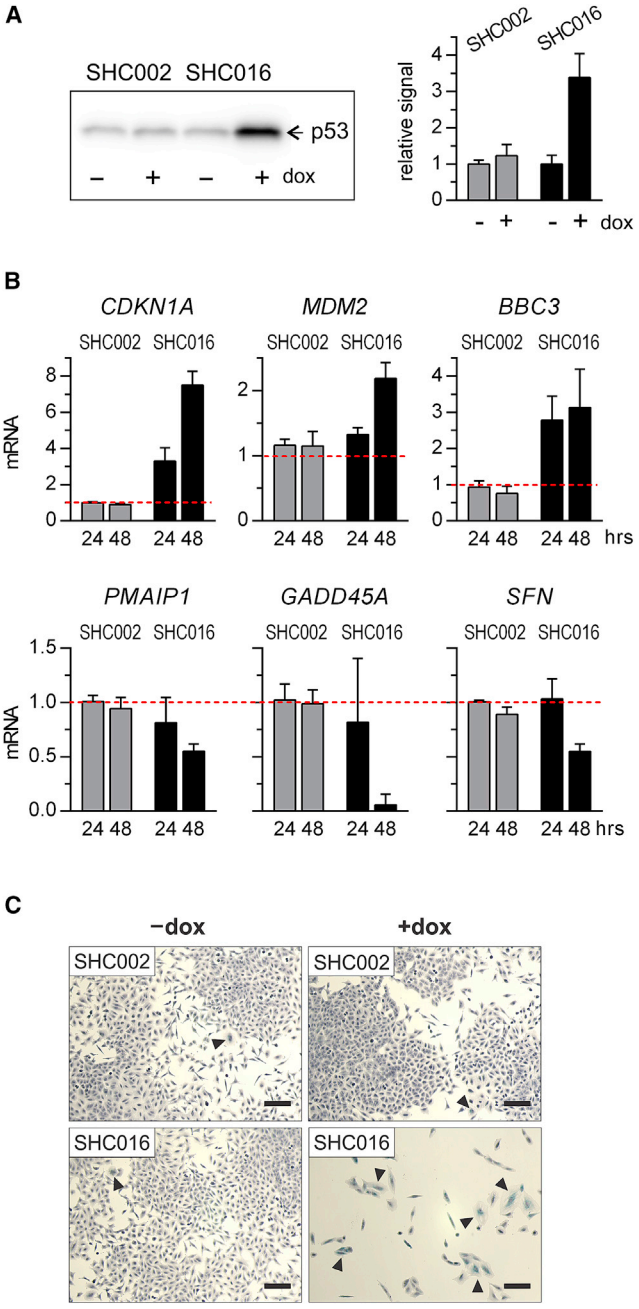

Figure 3. Expression of SHC016 in A549 cells initiates cell senescence

(A) WB analysis of p53 levels in A549 cells incubated for 48 h with or without dox. A representative image and quantification of WB signals of three independent experiments are shown. Luminescent signals were collected for ~40 s. The images of whole WB and Ponceau S-stained membrane are given in Figure S9. (B) qRT-PCR analysis of mRNA levels of p53 target genes. The cells were incubated for 1 or 2 days with or without dox. The relative levels of the transcripts in uninduced cells were taken as 1. MV ± SD from 3 independent experiments is shown. (C) Representative images of A549 cells stained for SA-β-gal activity and counterstained with hematoxylin. The cells were left untreated, or the expression of SHC002 or SHC016 was induced with dox 5 days prior to staining. Exemplary SA-β-gal-positive cells, very rare among untreated and cells expressing SHC002 but common among cells expressing SHC016, are indicated by arrowheads. The scale bar represents 100 μm. Three independent experiments were performed.

and drives cells to an irreversible fate (death or senescence).[17] This process occurs when defective checkpoints do not arrest cell-cycle progression in response to critical conditions such as genotoxic stress, delayed DNA replication, or aberrant spindle formation.

Giant multinucleated cells that are typical of MC comprised a considerable proportion of the U251 and PC3 cells expressing SHC016 (Figures 4A and 4B and S12). Some giant nuclei continued to synthesize DNA at 5 days after switching to SHC016 expression. The findings of fluorescence microscopy showed that BrdU was incorporated into DNA when added at the end of U251 culture (Figure S13). This agreed with the cytometric analysis of cell proliferation and viability, which showed that ~32% of U251 cells expressing SHC016 incorporated BrdU (Figure 2B). However, BrdU was not always evenly distributed within DNA, indicating unsynchronized DNA replication in some U251 cells expressing SHC016 (Figure S13).

The images of interphase nuclei of cells expressing SHC016 also revealed irregular patches of heterochromatin (another trait of necrosis and senescence), numerous micronuclei, and occasional supernumerary centrosomes (Figures 4C and S14). Multipolar spindles were formed during metaphase more often in U251 cells expressing SHC016 than SHC002 and also in these cell lines when cultured without doxycycline. Almost 25% of mitotic cells expressing SHC016 formed multipolar spindles, whereas in other groups, such a defect was observed in ~5% of mitotic cells. Chromosome alignment was also occasionally defective in U251 cells with induced SHC016 expression (Figures 4D and 4E).

We analyzed the expression of genes encoding proteins involved in cell-cycle execution and control, including those responsible for correct spindle formation. The results showed that SHC016 expression in U251 cells did not significantly affect the levels of most transcripts for at least up to 48 h after doxycycline induction (Figure S15). Like the other cell lines examined, levels of both *SFN* and *GADD45A* transcripts decreased in response to SHC016 expression in U251 cells. The effects of SHC016 expression in studied cells are summarized in Table S2.

To verify the hypothesis that the type of cell death induced by SHC016 expression depends on p53 status, we knocked down *TP53* in A549 cells (Tet-on-SHC002 and Tet-on-SHC016 transduced) using the CRISPR-Cas system. We then compared the effects of SHC016 expression in p53-WT and p53-knockdown (p53-KD) A549 cells. Western blots showed that the accumulation of p53 in response to SHC016 expression was impaired in p53-KD, compared with p53-WT A549 cells (Figure 5A). The substantial decrease in p53 inducibility did not change the SHC016-mediated decline in A549 viability (Figure 5B). However, the appearance of nuclei of SHC016-expressing p53-WT and p53-KD cells significantly differed

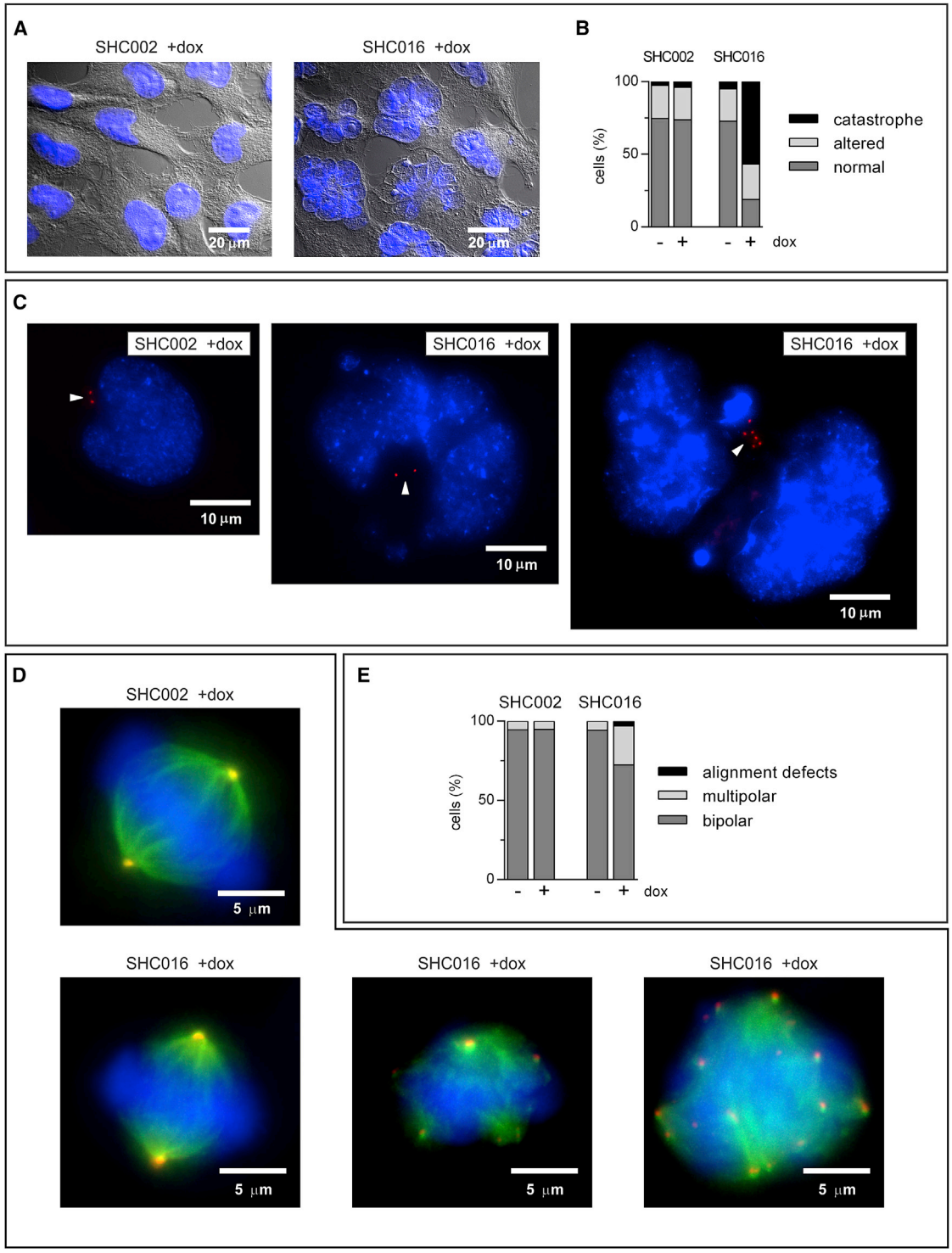

Figure 4. Expression of SHC016 in U251 cells results in mitotic catastrophe

Fluorescence microscopy analyses of nuclear morphology and mitosis in U251 cells. The cells were left untreated, or the expression of SHC002 or SHC016 was induced with dox 5 days prior to DNA staining. (A) Exemplary merged transmitted light and fluorescence images representing U251 with regular nuclei typical for SHC002-expressing cells or U251 with catastrophic nuclei prevailing among cells expressing SHC016. DNA was stained with DAPI (blue). Original images are available in Figure S12A. More examples are presented in Figure S12B. (B) Quantitative analysis of nuclear morphology in U251 with uninduced or induced expression of SHC002 or SHC016. Data are from two

(legend continued on next page)

(Figures 5C and 5D and S17). The fraction of cells with altered nuclear morphology (irregularly shaped nuclei or micronuclei) was substantially greater in p53-KD A549 cells with induced SHC016 shRNA expression than in p53-WT cells expressing SHC016 (49% versus 26%). Moreover, unlike p53-WT A549 cells, 20% of p53-KD A549 cells were driven toward MC after switching on SHC016 expression with doxycycline (Figures 5C, 5D, and S17)S17. The morphological abnormalities were similar among p53-KD A549 cells and U251 and PC3 p53 mutant cells expressing SHC016, supporting the notion that p53 status influences the mode of SHC016-induced death or growth arrest in human cell lines.

Changes in the expression of genes important for cell-cycle progression differed among cell lines. Therefore, we rejected the notion that these genes are responsible for the SHC016-induced effects. We conducted a preliminary RNA sequencing (RNA-seq) analysis of RNA from two cell lines to identify the primary mediator(s) of these effects. We analyzed RNA isolated from A549 and U251 cells transduced with Tet-on-SHC016 and incubated for 24 h with or without doxycycline. Levels of cyclic AMP (cAMP)-regulated phosphoprotein 19 (*ARPP19*), vacuolar protein sorting B (*VPS4B*), and small nuclear ribonucleoprotein Sm D3 (*SNRPD3*) transcripts were substantially diminished in both cell lines after inducing SHC016 expression. Analysis using g:Profiler and published results indicated that the products of these transcripts regulate cell-cycle progression and cell division (ARPP19 and VPS4 proteins) or when downregulated, trigger activation of the p53 pathway or abnormal mitosis (SNRPD3). The activity of ARPP19, which is an inhibitor of PP2A phosphatase, is required to maintain high levels of cyclin B1-CDK1 complexes during mitosis.[18] VPS4B is a part of the ESCRT III complex involved in cytokinesis,[19] and SNRPD3 is a component of U1, U2, U4, and U5 Sm RNP (snRNP) complexes.[20]

To verify the importance of RNA-seq results, we analyzed the influence of SHC016 on *ARPP19*, *VPS4A*, *VPS4B*, and *SNRPD3* expression in the human cell lines and in murine MC38CEA cells. Although RNA-seq analysis revealed decreased *VPS4A* expression only in A549 cells, we included this gene because VPS4A is essential for proper spindle formation and cytokinesis,[19] processes that are seriously disturbed in U251 cells. The levels of *ARPP19*, *VPS4B*, and *SNRPD3* transcripts were decreased in all human cell lines in response to SHC016, but not to SHC002, and the decrease in *SNRPD3* was the most significant (Figures 6A and S18). The levels of *VPS4A* were diminished in response to SHC016 in all human cells except MCF7. Levels of *Arpp19* and *Vps4b* were not affected, *Vps4a* was moderately reduced, whereas *Snrpd3* expression was reduced by ~75% in murine MC38CEA cells expressing SHC016 (Figure S18).

To determine whether the decrease in the expression of any of these genes mimics the effects of SHC016, we applied a doxycycline-inducible CRISPRi system to A549 and U251 cells using two single guide RNAs (sgRNAs) to silence the transcription of each gene. We analyzed the effects of CRISPRi later than those of shRNAs because CRISPRi inhibits *de novo* RNA synthesis, whereas shRNA affects existing RNAs. Levels of specific mRNAs were measured at 72 h, and the effects on cell viability were assessed at 6 days after inducing dCas-KRAB-MeCP2 expression.

SNRPD3, *VPS4A*, *VPS4B*, and *ARPP19* transcript levels were moderately decreased when dCas9-KRAB-MeCP2 expression was induced in U251 cells by 100 ng/mL of doxycycline (Figure S19), whereas were decreased to ~50%, 40%, 25%, and 35%, respectively, of their initial levels by 1 μg/mL of doxycycline (Figures 6B and S19). Decreasing *SNRPD3* expression by 50% in U251 cells resulted in decreased cell viability (Figure 6B) associated with the hallmarks of MC found in U251 cells expressing SHC016 (Figure S20). Silencing *VPS4A*, *VPS4B*, or *ARPP19* did not affect the viability of U251 cells (Figure 6B).

The A549 cells were resistant to transfection, and attempts to efficiently silence the expression of all genes of interest via cell transfection with CRISPRi plasmids bearing one sgRNA sequence failed (Figure S21A). Simultaneous transfection of A549 cells with two CRISPRi plasmids encoding different gene-specific sgRNAs improved the outcome, but levels of *SNRPD3* and *VPS4A* transcripts were diminished by only ~30% (Figure S21A) when transfection was replaced by electroporation levels of silencing *SNRPD3*, and *VPS4A* reached ~50%, and *VPS4B* and *ARPP19* reached ~75% (Figure S21A). The decrease in the level of *SNRPD3* mRNA, but no other studied transcript, resulted in a substantial decline in A549 viability and an increase in *CDKN1* expression (Figure 6C). Even small reductions in *SNRPD3* mRNA levels after transfection of A549 cells with single or double CRISPRi plasmids were accompanied by diminished cell viability (Figure S21B).

We concluded that reduced levels of *SNRPD3* in response to SHC016 expression accounted for the processes that led to death or at least to the permanent growth arrest of various cells transduced with the

independent experiments; in each experiment, at least 120 cells were analyzed in each group. The population described as "altered" includes cells with significantly enlarged nuclei, nuclei with irregular shapes and blebs, and those with micronuclei. (C) Exemplary fluorescence images of interphase nuclei of cells expressing SHC002 or SHC016. DNA was stained with Hoechst 33342 (blue). Arrowheads point out pairs of centrosomes (left and middle images) or supernumerary centrosomes (right image) visualized by γ-tubulin immunostaining (red). More images are available in Figure S14. (D) Exemplary fluorescence images of metaphase in U251 cells. Left images present correct number and position of centrosomes and correct formation of the spindle and metaphase plate; remaining images show an aberrant number of centrosomes and metaphase plate formation. Spindle microtubules were visualized by β-tubulin immunostaining (green), centrosomes were visualized by γ-tubulin immunostaining (red), and DNA was stained with Hoechst 33342 (blue). The scale bar represents 20 μm in (A), 10 μm in (C), and 5 μm in (D). (E) Quantitative analysis of correct and aberrant metaphase in U251 cells. The cells were left uninduced or were dox induced to express SHC002 or SHC016 2 days before analysis. Data are from three independent experiments. The total number of metaphase nuclei analyzed in each experimental group was ~160.

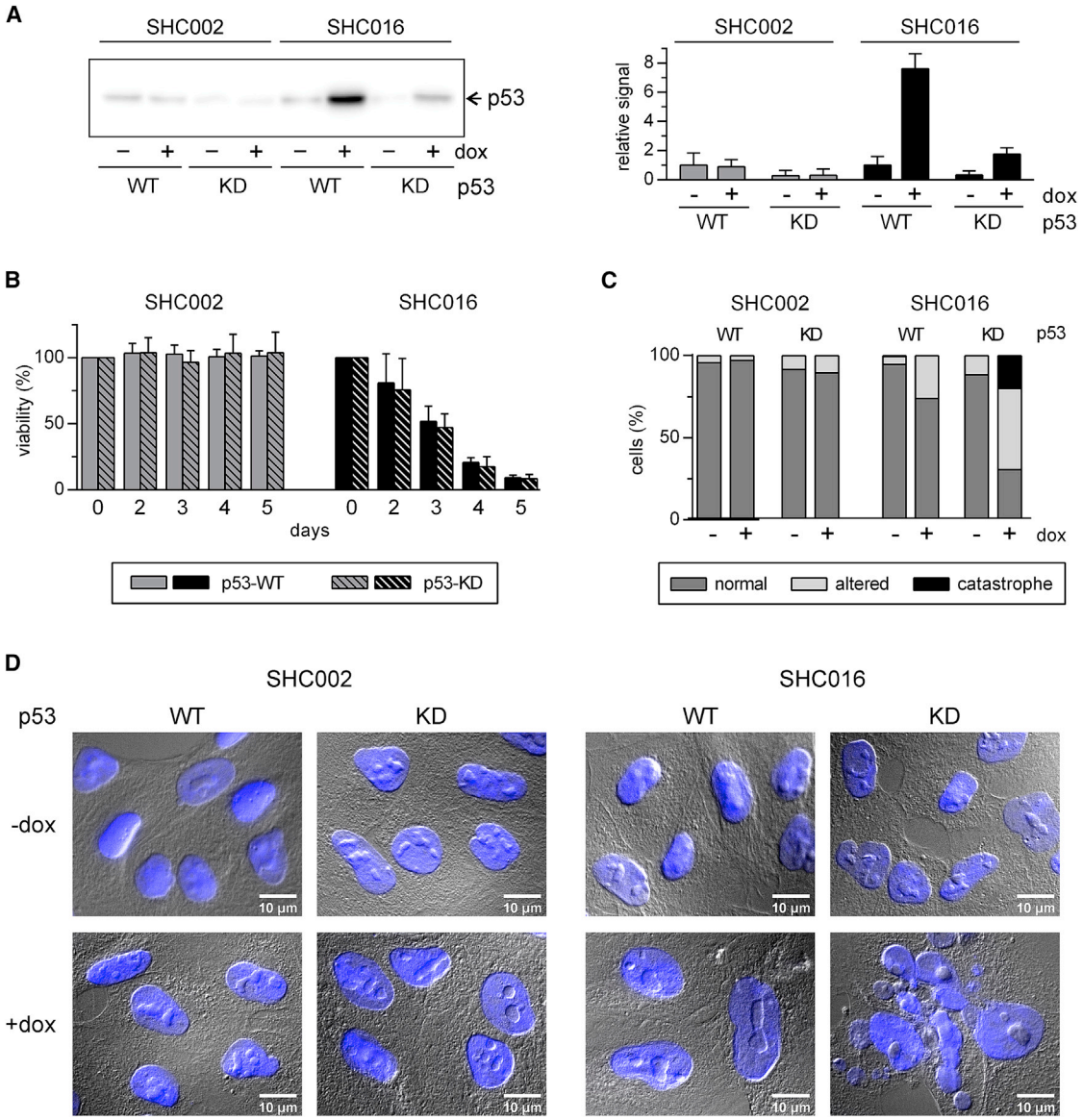

Figure 5. *TP53* knockdown (KD) in A549 cells promotes mitotic catastrophe in response to SHC016 expression

(A) WB analysis of p53 levels in the lysates of p53-wild-type (WT) and p53-KD A549 cells in which SHC002 or SHC016 expression was induced by dox (100 ng/mL) 2 days prior to cell lysis. Right panel: quantification of normalized WB signals; p53-linked luminescence signals of the samples from p53-WT, dox-untreated cells were set as 1. Bars represent MV ± SD from 3 independent experiments. The uncropped WB image and the picture of Ponceau S-stained membrane are available in Figure S16. (B) Cell viability assessed by MTT assay. The expression of SHC002 or SHC016 was induced by dox for the last 5, 4, 3, or 2 days of the 6-day culture. Bars represent MV ± SD from 4 independent experiments. (C) Quantitative analysis of nuclear morphology of p53-WT and p53-KD A549 cells visualized by fluorescence microscopy. The cells were left untreated, or the expression of SHC002 or SHC016 was induced with dox 5 days prior to DNA staining with Hoechst 33342. The population described as altered includes cells with irregularly shaped nuclei, those with nuclear blebs or micronuclei, and binucleated ones. Data are from one experiment representative of three independent experiments with similar results. At least 150 cells were analyzed for each experimental group. (D) Exemplary merged transmitted light and fluorescence images of p53-WT and p53-KD A549 cells. Induction of SHC016 expression resulted in mitotic catastrophe only in p53-KD cells (last image, lower panel). DNA was stained with Hoechst 33342 (blue). The scale bar represents 10 µm. Original images are available in Figure S17A. More examples are presented in Figure S17B.

MISSION non-targeting SHC016 vector. Because SNRPD3 is a subunit of the Sm protein complex involved in splicing, we speculated that a deficiency results in defective *VPS4A*, *VPS4B*, or *ARPP19* transcript splicing and a decrease in the levels of these mRNAs. However, CRISPRi-diminished expression of *SNRPD3* was accompanied by slightly increased levels of *VPS4B* and *ARPP19* transcripts in U251 cells. In contrast, the levels of *VPS4A* were moderately reduced upon *SNRPD3* silencing (Figure S22).

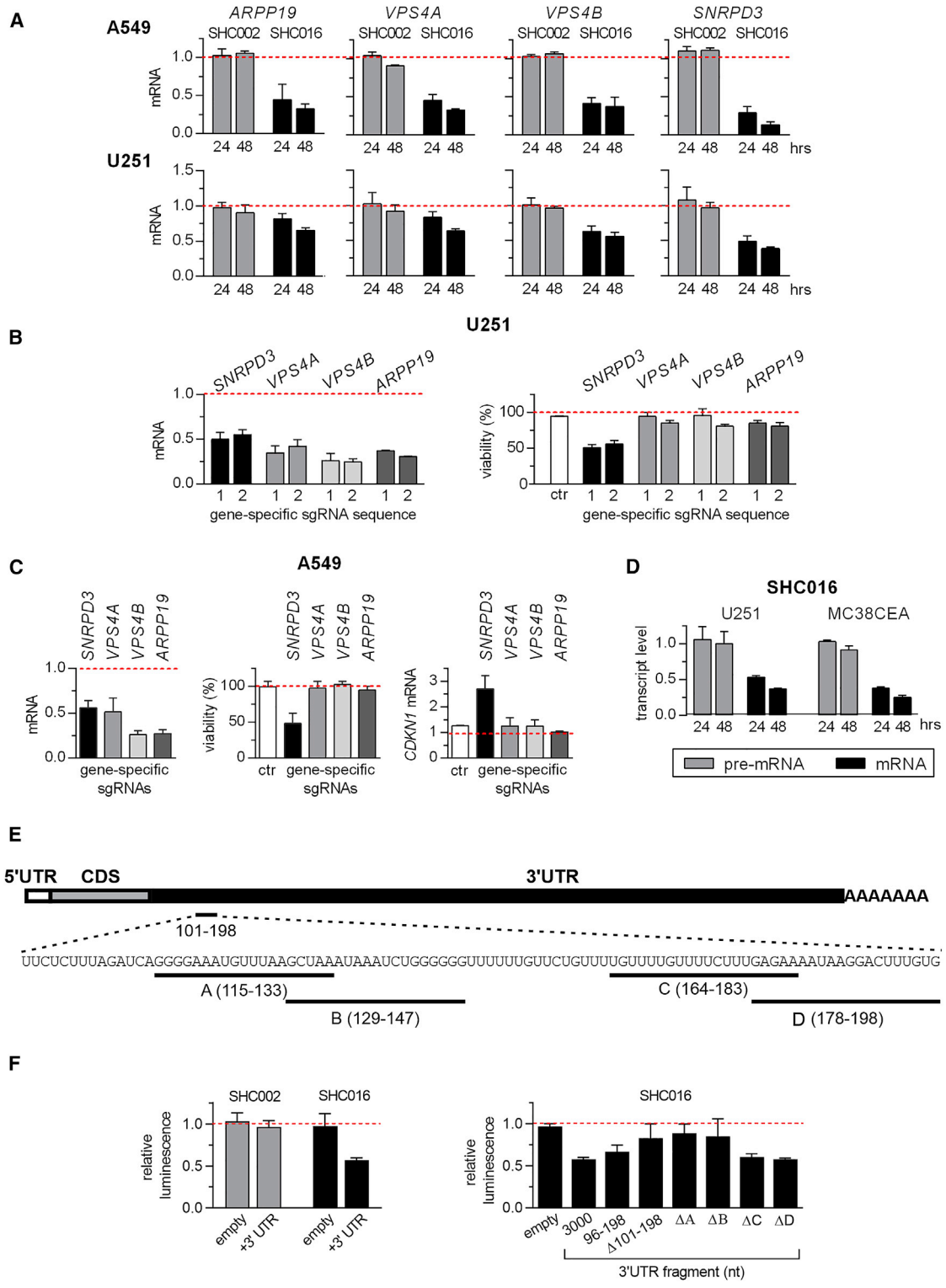

Figure 6. Deleterious effects of SHC016 are caused by diminished *SNRPD3* transcript levels

(A) qRT-PCR analysis of transcripts identified by RNA-seq as potentially affected by SHC016 performed 24 and 48 h after inducing expression of SHC002 or SHC016 shRNAs in A549 and U251 cells. The relative levels of the transcripts in uninduced cells were taken as 1. The data concerning other cell lines are available in Figure S18. (B)

(legend continued on next page)

We next investigated the mechanism through which SHC016 caused the decrease in *SNRPD3* transcript levels. In contrast to the diminished levels of a mature *SNRPD3* transcript, SHC016 expression did not affect its pre-mRNA levels in U251 and MC38CEA cells, indicating that SHC016 did not interfere with *SNRPD3* transcription but rather acted at the post-transcriptional level (Figure 6D). We applied the luciferase reporter assay to determine whether the susceptibility of the *SNRPD3* transcript to SHC016-mediated effects depended on its 3′ UTR. We cloned the human *SNRPD3* (*hSNRPD3*) 3′ UTR (Figure 6E) into the pmirGLO vector, which enabled estimation of the effect of *SNRPD3* 3′ UTR on luciferase activity after switching on SHC002 or SHC016 expression. In U251 cells transfected with an empty vector (without *SNRPD3* 3′ UTR) or with a vector carrying the *SNRPD3* 3′ UTR, luciferase activity did not change after inducing SHC002 expression. The induction of shRNA expression reduced the luciferase activity in the U251 transduced with SHC016 and transfected with pmirGLO containing *SNRPD3* 3′ UTR. The absence of changes in the cells transfected with the empty vector indicated that the *SNRPD3* 3′ UTR was responsible for the diminished luciferase activity after inducing SHC016 expression (Figure 6F). Analysis of SHC016-mediated inhibition of luciferase activity in U251 cells transfected with vectors encoding luciferase CDS with *SNRPD3* 3′ UTR-derived fragments of various lengths revealed that a sequence comprising nucleotides (nt) 100−200 of the 3′ UTR might be involved in the SHC016-mediated downregulation of *SNRPD3* mRNA (Figures 6F and S23B and S23C).

U251 cells transfected with pmirGLO vector containing nt 96−198 of the *SNRPD3* 3′ UTR showed almost the same reduction in luciferase activity after switching on SHC016 expression as the cells transfected with pmirGLO containing full-length *SNRPD3* 3′ UTR (Figure 6F). In contrast, luciferase activity was only slightly decreased when pmirGLO carried the *SNRPD3* 3′ UTR lacking nt 101−198 (Δ101−198). This indicated that SHC016 targets a sequence that lies within nt 101−198 of the *SNRPD3* 3′ UTR. We then performed analysis of potential interactions between sequences possibly derived from precursor SHC016 shRNA and the fragment of *SNRPD3* 3′ UTR (nt 101−198) using RNAhybrid.[21] Because shRNAs derived from pLKO1 vectors are known to undergo Dicer-independent processing, we analyzed every possible 21 nt sequence derived from SHC016. We then deleted fragments in the pmirGLO-*SNRPD3* 3′ UTR that were the most probable sites of interaction with shRNA-derived sequences based on the lowest free energy of binding (the sequences and locations of the deleted regions are shown in Figure 6E). Deletions of sites A and B (ΔA and ΔB, respectively) considerably diminished the negative effects of SHC016 expression on luciferase activity. Possible interactions between SHC016-derived sequences and SNRPD3 3′ UTR are presented in Figure S23D. Luciferase activity in U251 cells transfected with Δ101−198, ΔA, and ΔB mutant plasmids was not fully restored. Inhibition of luciferase activity was lower when pmirGLO contained nt 96−198 of the *SNRPD3* 3′ UTR instead of the full-length 3′ UTR. Therefore, we suspect that *SNRPD3* 3′ UTR might have additional, low-affinity sites of interaction with sequences derived from SHC016 shRNA. The same sequences derived from SHC016 might bind to the mouse *Snrpd3* (*mSnrpd3*) transcript mediating its downregulation (Table S3).

To verify the hypothesis that silencing SNRPD3 is the key mediator of SHC016-induced deleterious effects, we transfected U251 cells carrying dox-inducible SHC002 or SHC016 shRNAs with vectors carrying *mSnrpd3*, *hSNRPD3*, and optimized (*opt-SNRPD3*) variants of *SNRPD3* CDS. All variants encoded the same amino acid sequence. Silent mutations were introduced at all possible sites in *opt-SNRPD3* to ensure that the new sequence was resistant to possible SHC016-mediated silencing. Transfecting U251 cells with either mouse or opt sequences allowed discrimination between endogenous and overexpressed *SNRPD3* transcripts, whereas transfection with the human sequence enabled evaluations of endogenous and total *SNRPD3* mRNA levels. The expression of SHC016 induced by doxycycline (100 ng/mL) for 48 h diminished levels of endogenous *SNRPD3* mRNA in U251 cells transfected with a control vector encoding EGFP and in U251 cells transfected with vectors carrying any of the SNRPD3-coding sequences (Figure 7A). The effects of 10 ng/mL of doxycycline were delayed but comparable after 96 h to those of a 2-day high dose of doxycycline. In contrast to endogenous *SNRPD3* mRNA, the expression of SHC016 did not affect levels of *SNRPD3* mRNAs transcribed from any of the introduced vectors (Figure 7A), implying that *SNRPD3* CDS is not a target of SHC016. Despite strong *SNRPD3* overexpression at the transcript levels judged by a comparison of ΔCq values in qPCR analysis (for example, ΔCq [*SNRPD3-EF2*] was −1.18, −2.87, and −3.07 for mouse, human, and opt sequences, respectively), the increase in protein levels was moderate even in the absence of SHC016. This was most probably due to a

The analysis of extents of *SNRPD3*, *VPS4A*, *VPS4B*, and *ARPP19* silencing and viability of U251 cells in which expression of particular genes was diminished by CRISPRi using two different sgRNAs for each gene (designated as 1 and 2; the sequences are presented in Table S5). Detailed data concerning the results of gene silencing are presented in Figure S19. (C) The analysis of extents of *SNRPD3*, *VPS4A*, *VPS4B*, and *ARPP19* silencing in A549 cells in correlation with cell viability (assessed by MTT) and *CDKN1* expression (assessed by qRT-PCR). Two sgRNAs (1/2) were used simultaneously in CRISPRi-mediated gene silencing. (B and C) MTT was performed on the 6th day after inducing dCas-KRAB-MeCP2 expression. Ctr, control cells transfected (U251) or electroporated (A549) with an empty CRISPRi plasmid (pSBtet-Pur-dCas9-KRAB-MeCP2-hU6-SapI), which does not contain a sequence coding for any gene-targeting sgRNA. (B and C) RNA was isolated 72 h after inducing dCas-KRAB-MeCP2 expression. (D) Comparison of *SNRPD3* (*Snrpd3*) pre-mRNA versus mRNA levels in U251 and MC38CEA cells 24 and 48 h after switching on expression of SHC016. The lack of effect of SHC002 is documented in Figure S23A. (A−D) The relative levels of the transcripts in uninduced cells were taken as 1. MV ± SD from three independent experiments is shown. (E) Illustration of *SNRPD3* transcript with marked sequences that were deleted. (F) Relative chemiluminescence signals in U251 cells transfected with pmirGLO vectors: (1) containing luciferase CDS without *SNRPD3* 3′ UTR (empty); (2) containing luciferase CDS followed by full-length (3,000 nt) *SNRPD3* 3′ UTR or full-length *SNRPD3* 3′ UTR with deleted fragments: 96−198 nt (Δ96−198), 115−133 (ΔA), 129−147 (ΔB), 164-183 (ΔC), and 178−198 (ΔD); and (3) containing luciferase CDS followed by a WT *SNRPD3* 3′ UTR fragment 101−198 nt. The luminescence signal of the cells, in which expression of SHC002 or SHC016 was induced with dox (100 ng/mL), is presented in relation to the signal of uninduced cells (taken as 1). MV ± SD from three (left panel) or two (right panel) independent experiments is shown.

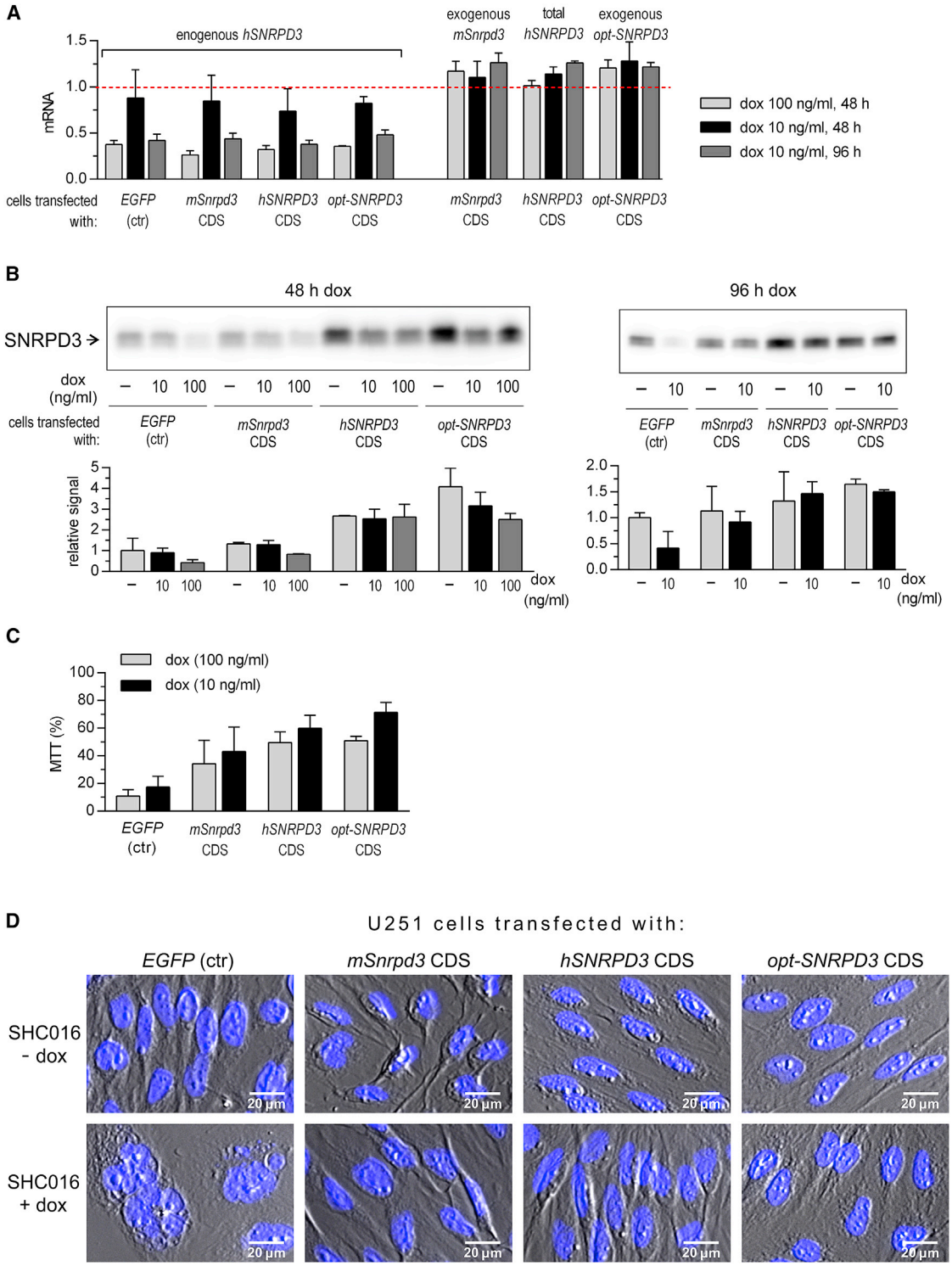

Figure 7. Restoring the expression of SNRPD3 in U251 cells reduces the deleterious effects of SHC016

(A) qRT-PCR analysis of *SNRPD3* mRNA levels in U251 cells transfected with a vector coding for EGFP (control) or a vector carrying one of the *SNRPD3*-coding sequences: mouse (*mSnrpd3*), human (*hSNRPD3*), or optimized (*opt-SNRPD3*) and treated with dox to induce SHC016 expression. The relative levels of the transcripts in uninduced cells were taken as 1. Data are shown as MV ± SD from two independent experiments. (B) WB analysis of SNRPD3 levels in U251 cells described in (A) incubated for 48 or 96 h with

(legend continued on next page)

mechanism that ensures a balanced supply of subunits of heteromeric complexes and involves the degradation of overproduced subunits relative to other proteins of the complex.[22,23]

The decrease in SNRPD3 protein in response to SHC016 expression in U251 cells transfected with a control vector reflected changes in mRNA levels. Doxycycline (100 ng/mL for 2 days or 10 ng/mL for 4 days) caused a substantial decrease of SNRPD3 in cells transfected with the control vector (Figure 7B). The level of endogenous SNRPD3 protein that was reduced in U251 cells expressing SHC016 was fully restored by the expression of exogenous *hSNRPD3* and *opt-SNRPD3* but only partially complemented by that of *mSnrpd3* (Figure 7B).

Cell viability determined using MTT assays was considerably improved in cells in which SHC016 expression was accompanied by exogenous SNRPD3 expression. The level of improvement correlated with that of SNRPD3 expression (Figures 7B and 7C). The restoration of efficient SNRPD3 synthesis abrogated the effect of a 24-h induction of SHC016 expression (Figure S25). Transfecting U251 with a vector encoding the *mSnrpd3*, *hSNRPD3*, or *opt-SNRPD3* variants rescued the cells from MC. Nearly all U251 cells transfected with the control EGFP-coding vector underwent MC after expressing SHC016 for 7 days. In contrast, MC was not evident in U251 with restored levels of SNRPD3 (Figures 7D and S26).

How is it possible that scientists around the world widely use the MISSION system without noticing the effects we describe here? Usually, commercially available vectors with non-inducible expression of shRNAs are used with the MISSION system. Therefore, the initial massive death of cells is attributed to the effects of puromycin on non-transduced cells. We believe that with subsequent cell divisions, only cells with low SHC016 expression survive, even when cells transduced with a vector encoding doxycycline-inducible SHC016 discontinuing the selective antibiotic puromycin, which is in line with generally accepted protocols, resulted in less deleterious effects of SHC016 compared with cells in which SHC016 was induced with doxycycline in the presence of puromycin. The viability of MCF7 and HeLa cells, evaluated using MTT assays, was further reduced by ~20% points, when cells expressing SHC016 were cultured for 5 days with puromycin (Figure 8A). Adding puromycin to the culture medium of HeLa cells also resulted in the increase in the population of dead cells, increasing from 5% to 40% in cells expressing SHC016 but not SHC002, according to the results of the proliferation and viability determinations (Figure 8B).

To verify the hypothesis that only cells with low SHC016 expression can persist in long-term cultures, we transduced MC38CEA and U251 cells, with uninducible, original versions of MISSION control vectors: namely, the empty vector SHC001 and two vectors with constitutive expression of the non-targeting shRNA sequences, SHC002 and SHC016. We isolated DNA from the cultured cells 2 days after transduction and then at 1-week intervals and analyzed levels of the transgenes by PCR using a primer pair that amplified the sequence comprising the PGK promoter and puromycin-resistance gene and another that amplified the area flanking the shRNA cloning site. Puromycin was added 48 h after transduction, and the cells were maintained under selective pressure for 7 days. The high mortality rate of U251 cells transduced with pLKO-SHC016 did not allow analysis within 1 month after transduction. Levels of SHC002 and SHC016 cassettes were similar at 2 days after transduction in both cell lines. However, in contrast to the empty vector and pLKO-SHC002, levels of the transgene containing SHC016 decreased dramatically during cell propagation (Figure 8C).

DISCUSSION

The initial enthusiasm accompanying the increasing application of RNAi techniques for exploring gene functions has recently declined with the emergence of publications highlighting their drawbacks and limitations, such as inefficient silencing of target gene expression, which could lead to false-negative results and false-positive off-target effects that are much more dangerous in terms of the further use of research results.[24] Jackson et al.[25], in the already "classic" publication, demonstrated that different siRNAs targeting the same transcript have unique global gene-expression profiles with only a few genes regulated in common. This could have far-reaching, disastrous consequences because RNAi-based studies are often the cornerstones for the development of novel therapies. The excellent study by Sheltzer's group[26] provided crushing evidence for misdirected drug development based on erroneous RNAi data that have led to failed clinical trials. They analyzed five proteins (HDAC6, mitogen-activated protein kinase 14 [MAPK14], PAK4, PBK, and PIM1) that had been selected based mostly on RNAi data, as those required for the survival and/or proliferation of cancer cells and for which small molecule drugs that specifically block their effects were already in clinical trials or preclinical studies. Using CRISPR-based techniques, the authors proved that neither knockout (via CRISPRko) nor reducing expression levels (via CRISPRi) of genes encoding these proteins affected the viability of 32 cancer cell lines. These genes were apparently wrongly selected, probably due to RNAi off-target effects. An OTS964 inhibitor selected as an inhibitor of one of these targets, namely PBK, exerted potent antimitotic effects but inhibited the kinase CDK11B. Thus, a completely different group of cancer patients should comprise the targets for treatment with this compound than was apparent according to RNAi-based studies.[26,27]

or without dox. Representative images and quantifications of WB signals (MV ± SD) of two independent experiments are shown. Whole WB and Ponceau S-stained membranes are given in Figure S24. (C) Cell viability of U251 cells described in (A) assessed by MTT assay. The cells were cultured for 7 days in the presence of dox to induce SHC016 expression. Absorbance values of the cells without induction of SHC016 expression were taken as 100%. Data are shown as MV ± SD from four independent experiments. Data parallel to these presented in (A)–(C) concerning U251 cells expressing SHC002 are presented in Figure S26. (D) Exemplary merged transmitted light and fluorescence images representing morphology of nuclei of U251 cells described in (A) cultured for 7 days with or without dox (100 ng/mL). DNA was stained with Hoechst 33342 (blue). The scale bar represents 20 μm. Low magnification images are available in Figure S27.

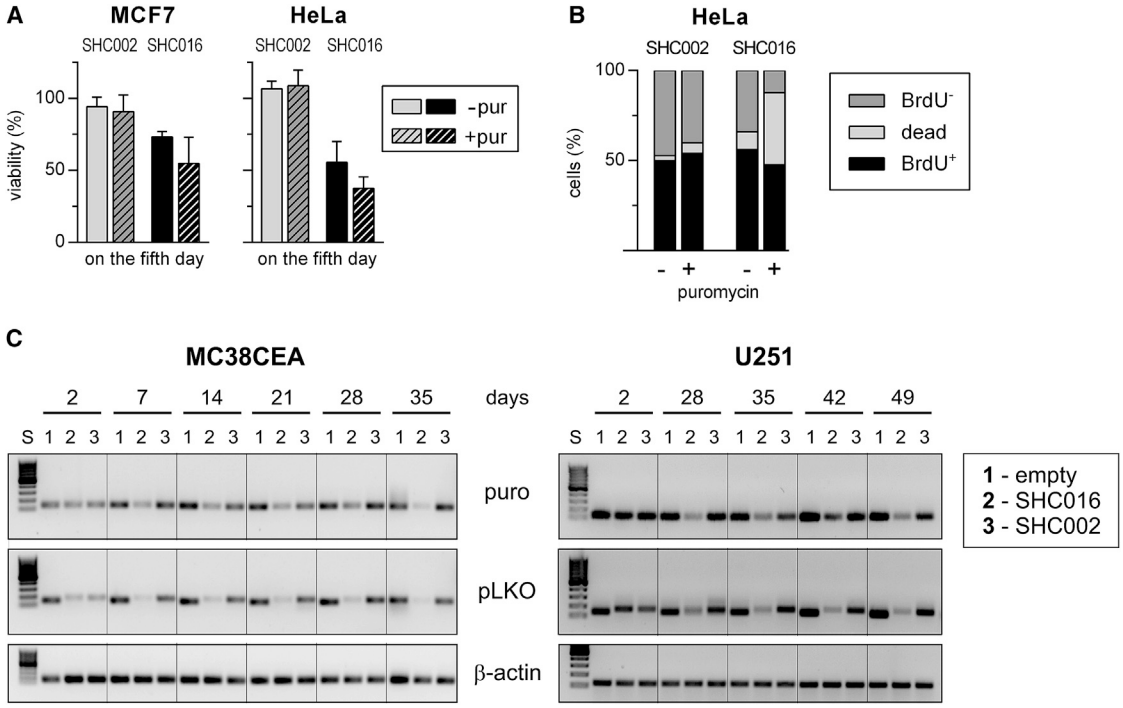

Figure 8. SHC016 expression cassette is eliminated from the cell cultures

(A) Comparison of the viability of MCF7 and HeLa cells 5 days after induction of either SHC002 or SHC016 shRNA expression in the absence or presence of selection antibiotic, puromycin (1 μg/mL), which was added for the last 72 h of culture. Absorbance values of the cells without induction of shRNA expression were taken as 100%. Data are shown as MV ± SD from 3 independent experiments. (B) Comparison of DNA synthesis and cell viability assessed via BrdU/eFluor 520 viability staining of HeLa cells expressing for 5 days either SHC002 or SHC016 in the absence or presence of selection antibiotic, puromycin. Dead, all eFluor 520$^+$ cells; BrdU$^+$, eFluor 520$^-$/BrdU$^+$ cells; and BrdU$^-$, eFluor 520$^-$/BrdU$^-$ cells. (C) PCR analysis of the abundance of the elements of pLKO vectors in the long-term cultures of MC38CEA and U251 cells. The cells were transduced with the empty vector (SHC001) or SHC002 or SHC016. DNA was isolated after indicated times, and the sequence from puromycin-resistance gene (puro) and the sequence comprising the shRNA insertion site (pLKO) were amplified. Inverted images of DNA electrophoresis gels are shown. S, size standard; GeneRuler 100 bp DNA Ladder, Thermo Scientific. The sizes of amplified fragments are as follows: puro, 123 bp; pLKO empty, 136 bp; and pLKO coding for either non-targeting RNA, 170 bp.

These examples and other critical analyses suggest that off-target effects might be erroneously attributed to the analyzed genes. Our work points to yet another overlooked and possible cause of discrepancies between various genotype-to-phenotype data and the frequent failure of verification of RNAi results by competitive or complementary techniques. The RNAi results might also be misinterpreted because of the off-target effects related to the non-targeting shRNA control, which, by definition, should not significantly affect the expression of any gene. We considered the consequences of the silencing activity of a non-targeting shRNA for RNAi data interpretation.

The first is that the inhibition of gene expression caused by a control shRNA, which functions as a reference, would be erroneously interpreted as the stimulation of the expression of that gene by experimental shRNAs.

However, the outcome of the control shRNA used in our study and probably in many others using MISSION shRNAs was more complex because SHC016 reduces the expression of the *SNRPD3* gene that is essential for cell survival. During post-transduction antibiotic treatment, the cells that were most likely to survive would have had strongly reduced expression of this toxic shRNA. Therefore, levels of non-targeting and targeting shRNAs are incomparable, and cells expressing non-targeting shRNA cease to function as appropriate controls.

Because shRNAs use miRNA processing machinery and compete with pre-miRNA for Dicer and Ago proteins,[28,29] disparate loads of shRNAs in control and experimental cells might distinctly influence endogenous miRNA functions, which would be manifested as differences in gene-expression profiles unrelated to specific shRNA effects. Moreover, during puromycin treatment, the cells that survive in the presence of antibiotic despite reduced occurrence of puromycin-resistance cassette associated with reduced levels of SHC016-coding sequence are selected. This functional phenotype can be attributed to cells overexpressing multidrug resistance gene(s) encoding ABC transporters that expel puromycin from cells.[30] Apart from differences in the expression levels of endogenous gene(s) rendering puromycin resistance, unmatched intracellular levels of transgenic puromycin *N*-acetyltransferase and/or puromycin itself might distinctly affect cell transcriptomes.[31]

Applying more restrictive rules for the design of control- and gene-specific shRNAs might limit off-target effects. The problem, however,

is quite complex due to the fact that the processing of the shRNA molecules, the choice of the guide strand from the siRNA duplex, and profiles of siRNA-mRNA interactions are not fully predictable.[2,4,32–39]

The recently discovered process of death induced by survival gene elimination (DISE) involves a group of siRNA/shRNAs that target the 3′ UTR of numerous essential survival genes via seed sequences as short as 6 nt.[38,40] This phenomenon might reflect the natural mechanism of action of tumor-suppressor miRNAs.[41] A similar mechanism has recently been proposed for viral miRNA-induced cell death.[42] However, SHC016 shRNA does not fit this scenario, as its sequence does not have the characteristics of those identified as the most toxic, and the RNA-seq analysis showed that the expression levels of the survival genes reduced in DISE were not substantially changed in response to SHC016 expression.

Our results indicated that SNRPD3 silencing is a major culprit responsible for SHC016-induced effects. snRNP D3 is one of core proteins of Sms, and it plays a pivotal role in all splicing steps. Given that >95% of human protein-coding transcripts are spliced, it is reasonable to expect that insufficient Sm core proteins would have global detrimental effects on cells and organisms. Accumulating evidence indicates that Sm core proteins, including SNRPD3, also influence the profile of alternative splicing.[43,44] We did not find a global reduction in transcript levels in response to *SNRPD3* silencing. Therefore, we suspected that the gradual decrease in this protein level primarily affects the expression of a few proteins crucial for cell-cycle progression.

SNRPD3 was selected in genomic screenings as one of the genes, depletion of which cause lethal defects in key steps of mitosis, including metaphase chromosome alignment[45] and sister chromatid cohesion.[46] However, little is known about possible transcripts encoding proteins crucial for cell-cycle progression, splicing of which might depend on SNRPD3 levels and whose defective splicing might explain the effects of silencing *SNRPD3* expression either unintentionally via SHC016 or purposely using CRISPRi.

One candidate is the centromere protein E (CENP-E) transcript. CENP-E, a plus-end-directed kinesin-7 motor protein participates in chromosome congression and microtubule-kinetochore conjugation as well as in activation of the spindle assembly checkpoint. A deficiency in this protein might lead to mitotic arrest, followed by cell death. Silencing SNRPD3 in DLD-1 and HCT116 colorectal cancer cell lines led to diminished *CENPE* expression.[47] We found that *CENPE* expression was diminished by ∼80% in A549 cells but only by ∼15% in U251 cells 48 h after inducing SHC016 expression (Figure S28). As *CENPE* is a DREAM target, the reduction of its mRNA level in A549 cells, the timing and extent of which resembles those of other DREAM-repressed genes, most probably results simply from p53 activation. The lack of a substantial decrease in *CENPE* mRNA in U251 cells 48 h after inducing SHC016 expression suggests that *CENPE* is not responsible for the early manifestations of MC triggered by *SNRPD3* silencing in U251 cells. However, because the estimated half-life of SNRPD3 (protein) is >27 h,[48] *CENPE* mRNA levels might become gradually reduced over time. Indeed, at early time points (48 h after induction), centrosome amplification seemed to be the culprit for MC in U251 cells, because defects in chromosome congression accounted for only a small proportion of all mitotic defects. However, centrosome staining 5 days after inducing shRNA expression revealed that only a portion of cells that had undergone MC had supernumerary centrosomes (Figures 4C and S14), indicating yet another mechanism that drives aberrant mitosis and in consequent MC.

SNRPD3 has also been identified in genome-wide screening of genes, silencing of which influences the viability of p53-WT cancer cells.[49] The authors showed that silencing several splicing factors, including SNRPD3, induces prominent p53 activation in A549 non-small cell lung cancer cells. Our findings of p53-p21 axis activation in A549 cells after SHC016 expression agree with these results. We found that SHC016- or CRISPRi-mediated silencing of *SNRPD3* resulted in deleterious effects in cells with or without active p53, which also agreed with the finding that cytotoxicity mediated by *SNRPD3* silencing does not depend on p53 activity. However, changes in *MDM4* splicing and expression postulated as a reason for deleterious effects of *SNRPD3* silencing[49] do not account for cytotoxicity in A549 and U251 in our studies, as we identified substantially diminished *Mdm4* mRNA levels in murine but not in human cells expressing SHC016 (Figure 1; data not shown). Thus, we postulate that at least in these cells, the altered splicing of transcripts other than *MDM4* plays crucial roles in mediating the effects of SHC016 expression and *SNRPD3* silencing. The transcript of structural proteasome subunit β3 (PSMB3) is defectively spliced in SNRPD3-deficient A549 cells, which might be a cause of cell lethality.[50] Additionally, aberrant splicing of the pre-mRNA coding for sororin, the regulator of sister chromatid cohesion, in cells depleted in SNRPD3 might be a key factor affecting mitosis in triple-negative breast cancer cells.[51] Considering the key role of SNRPD3 in splicing, many transcripts, including those encoding proteins important for cell survival and proliferation, are probably affected by incorrect alternative splicing.

MATERIALS AND METHODS

Cell line cultures

The following cell lines were used: MC38CEA (murine colon adenocarcinoma[52] expressing human carcinoembryonic antigen[53]), MEF (immortalized with SV40 LT, a gift from Prof. Paul Saftig, Christian-Albrechts University Kiel, Germany),[54] U251 MG (human glioblastoma, verified by Eurofins Medigenomics, Ebersberg, Germany), A549 (human lung carcinoma; ATCC CCL-185), PC3 (human prostate adenocarcinoma; ATCC CRL-1435), MCF7 (human breast adenocarcinoma; ATCC HTB-22), and HeLa (human cervical adenocarcinoma; ATCC CCL-2). HeLa cells were grown in MEM (Lonza, Basel, Switzerland) and all other cell lines in DMEM (Corning, Corning, NY, USA), supplemented with 10% heat-inactivated fetal bovine serum (FBS) and tetracycline negative (Capricorn Scientific, Ebsdorfergrund, Germany) at standard conditions. The cell cultures were routinely tested by PCR for mycoplasma contamination using mycoplasma rDNA-specific primers.

Lentiviral vectors

The following vectors from the MISSION library were used: MISSION pLKO.1-puro Empty Vector Control Plasmid DNA, which does not contain any shRNA insert (SHC001); MISSION pLKO.1-puro Non-Mammalian shRNA Control Plasmid DNA (SHC002), containing an shRNA insert, which, according to the description, does not target any known mammalian genes; and MISSION pLKO.1-puro Non-Target shRNA Control Plasmid DNA (SHC016), containing an shRNA insert, which, according to the description, does not target any genes from any species. SHC002 and SHC016 controls are available exclusively in the MISSION library. To produce doxycycline-inducible shRNA expression vectors, oligonucleotides coding for non-targeting shRNAs, identical to those in MISSION SHC002 and SHC016, 5′-CCGGCAACAAGATGAAGAGCACCAACTCGAGTTGGTGCTCTTCATCTTGTTGTTTTT-3′ and 5′-CCGGGCGCGATAGCGCTAATAATTTCTCGAGAAATTATTAGCGCTATCGCGCTTTTT-3′, respectively, were annealed and cloned into *Age*I/EcoRI-linearized tet-pLKO-puro (Addgene plasmid #21915, a gift from Dmitri Wiederschain).[55] Resulting vectors are referred to as Tet-on-SHC002 and Tet-on-SHC016.

Production and titration of lentiviral vectors

2 days prior to transfection, 293T cells were plated on 10 cm plates. The cells were transfected with plasmids: 1.3 pmol psPAX2 and 0.72 pmol pMD2.G (Addgene plasmids #12260 and #12259; both were gifts from Didier Trono) and 1.64 pmol respective pLKO plasmid using PEI MAX 40K (Polysciences, Warrington, PA, USA) at a ratio of DNA to PEI 1:3. Medium was changed 4 h after transfection. Cell culture supernatants containing pseudoviral particles were collected 48 h later, filtered through 0.45 μm PES filters, and concentrated by overnight centrifugation at 8,500 × *g*, 4°C. Pellets containing pseudoviral particles were resuspended in equal volumes of serum-free DMEM. Initially, vectors were titrated using the Quick-Titer Lentivirus Titer Kit (lentivirus-associated HIV p24; Cell Biolabs, San Diego, CA, USA). The viral titers for SHC002 and SHC016 were similar; therefore, in subsequent experiments, equal volumes of concentrated viruses were used.

Cell transduction

The cells were grown in a 12-well plate. An optimal volume of viruses was determined experimentally by transducing each cell line with several dilutions of a concentrated viral stock. Aliquots of 2 μL of stocks, which resulted in 20%–60% of puromycin-resistant cells, were eventually used for transduction of all cell types via spinoculation (30 min, 1,150 × *g*, room temperature) in the presence of polybrene (8 μg/mL). After 48 h, the transduced cells were selected for 7 days with puromycin (Bioshop Canada, Burlington, ON, Canada) at a concentration of 1 μg/mL for human cell lines, 5 μg/mL for MC38CEA, and 8 μg/mL for MEF.

PCR analysis of stability of transgene integration

MC38CEA and U251 MG (further referred to as U251) cells transduced with lentiviral vectors SHC001, SHC002, and SHC016 were cultured for several weeks. DNA was isolated from the cells at weekly intervals. The cells were lysed in guanidinium thiocyanate solution, and DNA was isolated by phenol-chloroform extraction.

Equal amounts of DNA samples (100 ng) were subjected to PCR using Taq Master Mix (Vazyme Biotech, Nanjing, China) to amplify the puromycin-resistance gene, puromycin N-acetyl-transferase, and a pLKO fragment comprising an shRNA-coding sequence, as well as an actin-coding sequence (*ACTB*/*Actb*) as a control. The primers are listed in Table S4. The PCR program included 30 cycles of 30 s at 94°C, 30 s at 60°C (human and mouse actin) or 52°C (puro and pLKO), and 30 s at 72°C. PCR products were visualized on a 1% agarose gel.

Stimulation of shRNA expression

The cells MC38CEA, MEF, U251, A549, PC3, MCF7, and HeLa transduced with Tet-on-SHC002 or Tet-on-SHC016 were seeded at a density appropriate for each cell line (between 500 and 1,500 cells/well in a 96-well plate or 10,000 and 20,000 cells/well in a 12-well plate). The cells were cultured for 5 or 6 days, and the cells of each line were divided into several experimental groups. Starting 1 day after plating of the cells, doxycycline aliquots were added every 24 h to one experimental group to a final concentration of 100 ng/mL (unless stated otherwise). One group (negative control) was left untreated. In some experiments, etoposide (2 μM) was added to one group for the last 48 h of culture as a positive control of apoptosis induction.

MTT assay

The viability of the cells was determined by MTT assay. The cells in 96-well plates were incubated in 100 μL of serum-free medium containing MTT (Sigma-Aldrich, St. Louis, MO, USA) at a concentration of 0.5 mg/mL for 1–3 h. Formazan crystals were solubilized in 200 μL of acidified isopropanol. The absorbance was measured at 570 nm using a microplate reader (VersaMax; Molecular Devices, San Jose, CA, USA). The absorbance of control cells (cultured without doxycycline) was taken as 100% viability.

Colony formation assay

The cells were seeded at 100 cells per well in a 6-well plate. On the following day, doxycycline was added at 100 ng/mL. The cells were cultured for 7–10 days, and fresh doxycycline was added every other day. At the 5th day, puromycin was added to select the cells that retained the expression cassette. The colonies were stained with crystal violet dissolved in methanol, destained with tap water, and photographed with a Fusion FX imaging platform (Vilber Lourmat, Collégien, France).

Annexin V assay

The cells were analyzed by an annexin V/PI double-staining method.[56] The cells with inducible SHC002 or SHC016 expression were grown in 12-well plates, and shRNA expression was induced with doxycycline as described above. The cells were trypsinized, washed with PBS and then with annexin V binding buffer (ABB; 10 mM HEPES, pH 7.4, 140 mM NaCl, 2.5 mM $CaCl_2$), and incubated in ABB containing annexin V conjugated with APC (1% v/v; Exbio,

Vestec, Czechia) and PI (100 μg/mL) for 20 min in the dark. Next, the cells were washed twice with ABB, resuspended in ABB, and analyzed on a FACSCalibur (BD Biosciences, San Jose, CA, USA). The percentages of apoptotic cells (annexin V positive, PI negative) and late apoptotic and necrotic cells (PI positive, annexin V positive and negative) were determined using FlowJo version (v.)10.0.7 (FlowJo, Ashland, OR, USA).

Measurement of caspase activity

MC38CEA and MEF cells with inducible SHC002 or SHC016 expression were seeded in 96-well plates, and shRNA expression was induced with doxycycline as described above. Caspase activity was determined using Caspase-Glo 3/7 Assay Systems (Promega, Madison, WI, USA) according to the manufacturer's specifications. The luminescence was measured using a microplate reader, Synergy H1 Hybrid Reader (BioTek, Winooski, VT, USA). The luminescence values of control cells, non-treated with doxycycline, were taken as 100%.

Cell-cycle analysis

The cells with inducible SHC002 or SHC016 expression were plated in 12-well plates at a density of 10,000 cells/well, and shRNA expression was induced with doxycycline as described above. The cells were trypsinized, washed with PBS, fixed with 70% ethanol, and incubated at 4°C for at least 4 h. Equal amounts of cells (1×10^5), were permeabilized with 0.1% Triton X-100 in PBS for 15 min, washed with PBS, and incubated in 200 μL of ribonuclease A (10 μg/mL; A&A Biotechnology, Gdynia, Poland) for 15 min at 37°C. Then 200 μL aliquots of PI dissolved in PBS containing 0.1% Triton X-100 were added to the cells to a final concentration of 250 μg/mL. The cell-cycle analysis of 10,000 cells/sample was performed by flow cytometry using FACSCalibur (BD Biosciences) and the FlowJo cell-cycle Watson (Pragmatic) model (FlowJo v.10.0.7 software; FlowJo). Both debris and doublets were removed from the analysis.

Nuclei imaging

The cells were washed twice with PBS, fixed with ice-cold methanol for 5 min, washed thoroughly with PBS, incubated with DAPI (1 μg/mL) or Hoechst 33342 (1 μg/mL) for 15 min, and washed 4 times with PBS. The nuclei were imaged using a Leica DM6 B microscope equipped with a Leica DMC5400 camera or a DM IL LED fluorescence microscope equipped with a Leica DFC450 C (Leica Microsystems, Wetzlar, Germany) camera, and the images were processed using ImageJ software v.1.53 (National Institutes of Health).[57,58]

Immunofluorescence

The cells were plated on #1.5 glass coverslips in 12-well plates. On the following day, doxycycline was added to a final concentration of 100 ng/mL, and 48 h later, the cells were washed with PBS, fixed with ice-cold methanol for 5 min, then washed three times with PBS, permeabilized with 0.5% Triton X-100 in PBS for 15 min at room temperature, blocked with 2% BSA and 5% normal goat serum in PBST (blocking solution) for 1 h, and incubated with mouse anti-γ-tubulin antibody (clone C-11, 2 μg/mL; Santa Cruz Biotechnology, Dallas, TX, USA), diluted in blocking solution overnight at 4°C. After washing with PBST, the coverslips were incubated with Fab fragment of goat anti-mouse immunoglobulin G (IgG; H+L) secondary antibody conjugated to Alexa Fluor 594 (Jackson ImmunoResearch, West Grove, PA, USA) for 1 h at room temperature. After extensive washing with PBST, the coverslips were subjected to mild fixation with 0.4% methanol-free formaldehyde in PBS for 10 min, washed with PBS, and incubated with CoraLite-488-conjugated mouse anti-β-tubulin antibody (clone 1D4A4, 10 μg/mL; Proteintech, Rosemont, IL, USA) in blocking solution overnight at 4°C. After washing with PBST, the coverslips were stained with Hoechst 33342 and mounted onto microscopic slides with ProLong Glass (Thermo Scientific). When the cells were stained for γ-tubulin only, the post-staining fixation step was omitted. The images were acquired with a Leica DM6 B microscope equipped with a Leica DMC5400 camera using a 63 × 1.3 NA oil objective. Images shown are maximum intensity projections of z stack planes.

BrdU labeling

The cells were seeded at a density of 20,000 cells/well (all but A549) or 60,000 cells/well (A549) in a 6-well plate. On the following day, doxycycline was added to a final concentration of 100 ng/mL. The cells (all but A549) were cultured for 5 days or 3 days (A549). Fresh doxycycline was added every other day. BrdU (Sigma-Aldrich), at a final concentration of 20 μM, was added to the medium for the last 6 h, and then the cells were collected, washed twice with PBS, and stained with Fixable Viability Dye eFluor 520 (Thermo Scientific, Waltham, MA, USA) in PBS for 30 min at 4°C with occasional mixing. To stop the reaction, the cells were washed once in 1% BSA/PBS and once in PBS. Then, the cells were fixed dropwise with ice cold 70% ethanol and incubated overnight at 4°C. On the next day, the fixed cells were subjected to DNA denaturation in 2 M HCl containing 0.5% Triton X-100 for 30 min at room temperature; HCl was neutralized with 0.1 M sodium tetraborate, pH 8.5. After extensive washes in PBS, the cells were incubated in blocking solution (1% BSA in PBST) for 20 min and then with Alexa Fluor 647-conjugated anti-BrdU antibody at 1:50 (clone MoBU-1; Thermo Scientific) for at least 3 h at room temperature. Next, the cells were centrifuged, suspended in PBS, and analyzed on a FACSCalibur (BD Biosciences). The percentages of BrdU-positive, BrdU-negative, and dead cells (Fixable Viability Dye eFluor 520 positive) were determined using FlowJo v.10.6.1 (FlowJo). In some experiments, U251 cells were also seeded on #1.5 glass coverslips and stained as describe above with minor modification (viability dye was omitted; staining was performed with Alexa Fluor 647- or Alexa Fluor 488-conjugated anti-BrdU antibodies). The samples were analyzed via fluorescence microscopy using a Leica DM6 B microscope equipped with a 63 × 1.3 NA oil objective and Leica DMC5400 camera (Leica Microsystems).

SA-β-gal staining

The cells were seeded 5 days prior to staining at 5,000 cells/well in 12-well plates, and shRNA expression was induced with doxycycline as described above. SA-β-gal staining was performed according to a standard protocol.[59] Briefly, the cells were washed twice with PBS,

fixed for 5 min with 2% formaldehyde and 0.2% glutaraldehyde in PBS, then washed in PBS, and incubated overnight at 37°C in staining solution containing 40 mM citric acid/sodium phosphate buffer, pH 6.0, 1 mg/mL X-Gal (Bioshop Canada), 5 mM potassium ferricyanide, 5 mM potassium ferrocyanide, 150 mM NaCl, and 2 mM $MgCl_2$. On the following day, the cells were washed with PBS, dehydrated in methanol, counterstained with hematoxylin, and washed extensively with water. The cells were imaged using a DM IL LED microscope equipped with a Leica DFC450 C camera. The percentage of SA-β-gal-positive cells was calculated. About 300 cells were analyzed per experiment in three independent experiments.

RNA isolation, reverse transcription, and qRT-PCR

Total RNA was isolated by the modified phenol/chloroform extraction method using a Fenozol reagent (A&A Biotechnology) and then treated with TURBO DNase (Thermo Scientific) followed by column purification with the Clean Up RNA Concentrator (A&A Biotechnology). Equal amounts of RNA (1 μg) were reverse transcribed with a mixture of oligo$(dT)_{15}$ and random hexamer primers using M-MLV polymerase (Promega). qRT-PCR gene expression quantifications were performed using AceQ qPCR SYBR Green Mix (Vazyme Biotech) on an Eco Real-Time PCR System (Illumina, San Diego, CA, USA). RNA expression was normalized to a geometric mean of two reference genes: *Eef2* and *Polr2b* for mouse cell lines and *EEF2* and *TBP* for human cell lines. All sequences of primers are listed in Table S4.

Preparation of samples for RNA-seq

Cells were seeded on 10 cm plates 2 days before doxycycline addition. After 24 h of doxycycline treatment, cells were lysed in RNA Extracol (EurX, Gdańsk, Poland). Total RNA was isolated using the Direct-zol RNA Mini (Zymo Research, Irvine, CA, USA); the procedure included on-column DNase I digestion. Poly$(A)^+$ fractions were isolated using the Dynabead mRNA DIRECT Micro Purification Kit (Thermo Scientific) according to the manufacturer's recommendations with minor modifications, such as three (instead of two) rounds of RNA binding, washing, and elution and an additional wash in detergent-free buffer B before the final elution step. Library preparations and sequencing on an Ion Torrent platform were performed at the Genomics Centre at the Malopolska Centre of Biotechnology (Kraków, Poland). The RNA-seq data presented in this article have been deposited in the GEO database (GEO: GSE178458). Reads per million mapped read values of samples treated with doxycycline and untreated were compared, and the transcripts that were downregulated in both cell lines were subjected to analysis in g:Profiler (https://biit.cs.ut.ee/gprofiler/gost).[60] Based on g:Profiler analysis and published results, transcripts encoding proteins involved in the regulation of the cell-cycle progression and cell division were selected for further analysis.

Generation of p53-KD A549 cells

Cas9 mRNA was transcribed from the *Xba*I-linearized pJET1.2-SpCas9 vector[61] using the HiScribe T7 ARCA mRNA Kit (with tailing) (NEB, Ipswich, MA, USA); mRNA was purified using LiCl precipitation. Oligonucleotides corresponding to the human *TP53*- or GFP-targeting portion of sgRNAs were cloned into pX330-U6-Chimeric_BB-CBh-hSpCas9.[62] sgRNA-coding sequences were amplified with primers containing a T7 promoter sequence at the 5′ end of the forward primer, purified using the Clean-Up Concentrator kit (A&A Biotechnology), *in vitro* transcribed using the TranscriptAid T7 High Yield Transcription Kit (Thermo Scientific), and then purified by LiCl precipitation. A549 cells were electroporated with 5 μg of Cas9 mRNA in electroporation buffer using Gene Pulser II (Bio-Rad Laboratories) under the following conditions: one million cells in 400 μL electroporation buffer in a 0.4-cm gap cuvette and pulse voltage and capacitance: 400 V and 700 μF. After 4 h, electroporation was repeated using the same procedure, but with 1 μg of *TP53*- or GFP-targeting sgRNAs instead of Cas9 mRNA. The cells were allowed to regenerate in culture (for about 3 days), and the electroporation was repeated with another *TP53*-targeting sgRNA (three in total). Sequences of oligonucleotides used for sgRNA cloning and for amplification of sgRNA for *in vitro* transcription are available in Table S5.

Construction of tet-inducible CRISPRi vector

dCas9 repressor was PCR amplified with primers containing *Sfi*I sites from dCas9-KRAB-MeCP2 (a gift from Alejandro Chavez and George Church; Addgene plasmid #110821),[63] digested with *Sfi*I, and cloned into an *Sfi*I-linearized pSBtet-Pur plasmid (a gift from Eric Kowarz; Addgene plasmid #60507).[64]

In order to clone the U6 promoter-sgRNA scaffold cassette containing *Sap*I restriction sites instead of *Bbs*I sites, oligonucleotides containing *Sap*I sites were annealed and cloned into the *Bbs*I-digested pX330-U6-Chimeric_BB-CBh-hSpCas9 (a gift from Feng Zhang; Addgene plasmid #42230).[62] The U6-sgRNA scaffold was then PCR amplified with primers containing KpnI sites and cloned into KpnI-digested pSBtet-Pur-dCas9- KRAB-MeCP2. The resulting vector was termed pSBtet-Pur-dCas9-KRAB-MeCP2-hU6-SapI.

sgRNA sequences targeting *hSNRPD3*, *VPS4A*, *VPS4B*, and *ARPP19* genes were designed using the GPP sgRNA Designer (Broad Institute). Oligonucleotides containing pSBtet-Pur-dCas9-KRAB-MeCP2-hU6-SapI-compatible ends were annealed and assembled with the vector in one restriction-ligation reaction with *Sap*I and the T4 DNA ligase. Sequences of oligonucleotides used for sgRNA cloning are available in Table S5.

U251 and A549 were seeded onto 12-well plates 1 day prior to transfection. The cells were transfected with 475 ng of a respective CRISPRi plasmid together with 25 ng of Sleeping Beauty transposase-encoding vector pCMV(CAT)T7-SB100 (a gift from Zsuzsanna Izsvak; Addgene plasmid #34879)[65] using jetOPTIMUS (A549 cells; Polyplus-transfection, Illkirch, France) or TransIT-LT1 (U251 cells; Mirus Bio, Madison, WI, USA), according to the protocols provided by the manufacturers. Alternatively, A549 cells were electroporated with 4.9 μg of CRISPRi plasmid and 100 ng of pCMV(CAT)T7-SB100 in electroporation buffer (100 mM sodium phosphate,

10 mM $MgCl_2$, 5 mM KCl, 20 mM HEPES, 50 mM sodium succinate, pH 7.2) using Gene Pulser II (Bio-Rad Laboratories, Hercules, CA, USA) under the following conditions: two million cells in 400 μL electroporation buffer in a 0.4-cm gap cuvette and pulse voltage and capacitance: 300 V and 1,000 μF. After 24 h of transfection, the medium was changed, and the transfected cells were selected for 7 days with puromycin at a concentration of 1 μg/mL for U251 cells and 5 μg/mL for MC38CEA cells.

Construction of SNRPD3 expression vectors

The sequences coding for *mSnrpd3* or *hSNRPD3* were amplified from cDNA synthesized from RNA isolated from mouse brain tissue or U251 cells, respectively. cDNAs were generated using Maxima H Minus Reverse Transcriptase (Thermo Scientific). The sequence coding for SNRPD3 with introduced, at every possible site, silent mutations (*opt-SNRPD3*) was synthesized as a dsDNA fragment (GeneArt Strings DNA Fragments; Thermo Scientific). EGFP was PCR amplified from LeGO-iG2 (a gift from Boris Fehse; Addgene plasmid #27341).[66] *mSnrpd3* and *hSNRPD3* were cloned into an *Sfi*I-linearized pSBbi-bla vector (a gift from Eric Kowarz; Addgene plasmid #60526)[64] using the NEBuilder HiFi DNA Assembly, whereas *opt-SNRPD3* and EGFP were digested with *Sfi*I and ligated into *Sfi*I-linearized pSBbi-bla.

U251 and MC38CEA were seeded onto 12-well plates 1 day prior to transfection. The cells were transfected with 950 ng of a respective pSBbi-bla-SNRPD3 plasmid together with 50 ng of transposase-encoding vector pCMV(CAT)T7-SB100[65] using ViaFect (U251 cells; Promega) at a ratio of DNA to reagent of 1:3 or jetPRIME (MC38CEA cells; Polyplus-transfection) at a ratio of DNA to reagent of 1:2. After 24 h, the medium was changed, and the transfected cells were selected for at least 10 days with blasticidin S (Invivogen, San Diego, CA, USA) at a concentration of 12 μg/mL for U251 cells and 5 μg/mL for MC38CEA cells.

Western blotting

The cells were incubated with or without doxycycline for 48 h and then lysed in ice-cold RIPA buffer enriched with 5 mM EDTA and Halt Protease Inhibitor Cocktail (Thermo Scientific). After brief sonication, protein samples (25 μg for 10-well gels or 15 μg for 15-well gels) were subjected to Tris-glycine SDS-PAGE (for the detection of p53) or Tris-tricine SDS-PAGE (for the detection of SNRPD3) and transferred onto 0.45 μm polyvinylidene fluoride (PVDF) or 0.22 μm nitrocellulose membranes (Immobilon P; Merck and Protran, Amersham, respectively). The membranes were stained with Ponceau S to ensure equal protein loading. After destaining and blocking in 5% non-fat dried milk in TBST, they were probed with goat-anti p53 at 0.25 μg/mL (AF1355; R&D Systems) or rabbit anti-SNRPD3 at 0.2 μg/mL (NBP1-80735, Novus Biologicals; or HPA001170, Sigma-Aldrich) and then with horseradish peroxidase (HRP)-conjugated secondary antibody (rabbit anti-goat or goat anti-rabbit, both at 1:10 000; Sigma-Aldrich). Bands were developed with Immobilon Western Chemiluminescent HRP Substrate (Merck) and visualized using Fusion FX (Vilber Lourmat). The exposition time was set to "auto." Band intensities were quantified using Fiji software;[58] chemiluminescent signal was normalized to the total protein amount in each lane visualized by Ponceau S staining.

Luciferase reporter assay

The sequence of *hSNRPD3* 3′ UTR was PCR amplified from cDNA synthesized from RNA isolated from U251 cells with primers containing *Xba*I restriction sites. The PCR product was cloned into pJET1.2/blunt (Thermo Scientific) and then subcloned into *Xba*I-linearized pmirGLO (Promega). Small deletions comprising potential shRNA-targeted sites within SNRPD3 3′ UTR were introduced using inverse PCR and pJET1.2-hSNRPD3 3′ UTR as a template; mutated versions of 3′ UTR were then subcloned into pmirGLO. Primers used for cloning and mutagenesis are available in Table S6.

U251 cells were seeded onto 96-well plates at 7,500 cells/well and transfected with 50 ng pmirGLO vectors using ViaFect (Promega) at a DNA to reagent ratio of 1:3. On the following day, the medium was changed, and doxycycline was added to a final concentration of 100 ng/mL. After 48 h, medium was removed, and activities of firefly and *Renilla* luciferases were determined using the Dual-Glo Luciferase Assay System (Promega).

Additional information

Data analysis was performed using Microsoft Excel (Excel 2016) or GraphPad Prism v.5, and all graphs were created using GraphPad Prism v.6 (GraphPad Software).

SUPPLEMENTAL INFORMATION

Supplemental information can be found online at https://doi.org/10.1016/j.omtn.2021.09.004.

ACKNOWLEDGMENTS

We thank Dr. Krystyna Stalińska and Ms. Olga Dracz for help in some experiments and Dr. Mateusz Wawro for critically reading the manuscript. This work was funded by the National Science Centre, Poland (NCN; OPUS11 funding scheme, project number UMO-2016/21/B/NZ3/00355 to J.B.). The open-access publication of this article was funded by the Priority Research Area BioS under the program "Excellence Initiative–Research University" at Jagiellonian University in Kraków.

AUTHOR CONTRIBUTIONS

M.C. and J.B. designed the study and wrote the article. M.C., K.S., and A.K. performed the experiments. M.C., K.S., J.K., and J.B. analyzed the data. All authors reviewed the results and approved the manuscript.

DECLARATION OF INTERESTS

The authors declare no competing interests.

REFERENCES

1. Shi, Y. (2003). Mammalian RNAi for the masses. Trends Genet. *19*, 9–12.
2. Gebert, L.F.R., and MacRae, I.J. (2019). Regulation of microRNA function in animals. Nat. Rev. Mol. Cell Biol. *20*, 21–37.

3. Paddison, P.J., Caudy, A.A., Sachidanandam, R., and Hannon, G.J. (2004). Short hairpin activated gene silencing in mammalian cells. Methods Mol. Biol. *265*, 85–100.
4. Sheng, P., Flood, K.A., and Xie, M. (2020). Short Hairpin RNAs for Strand-Specific Small Interfering RNA Production. Front. Bioeng. Biotechnol. *8*, 940.
5. Berns, K., Hijmans, E.M., Mullenders, J., Brummelkamp, T.R., Velds, A., Heimerikx, M., Kerkhoven, R.M., Madiredjo, M., Nijkamp, W., Weigelt, B., et al. (2004). A large-scale RNAi screen in human cells identifies new components of the p53 pathway. Nature *428*, 431–437.
6. Moffat, J., Grueneberg, D.A., Yang, X., Kim, S.Y., Kloepfer, A.M., Hinkle, G., Piqani, B., Eisenhaure, T.M., Luo, B., Grenier, J.K., et al. (2006). A lentiviral RNAi library for human and mouse genes applied to an arrayed viral high-content screen. Cell *124*, 1283–1298.
7. Paddison, P.J., Silva, J.M., Conklin, D.S., Schlabach, M., Li, M., Aruleba, S., Balija, V., O'Shaughnessy, A., Gnoj, L., Scobie, K., et al. (2004). A resource for large-scale RNA-interference-based screens in mammals. Nature *428*, 427–431.
8. Chang, K., Elledge, S.J., and Hannon, G.J. (2006). Lessons from Nature: microRNA-based shRNA libraries. Nat. Methods *3*, 707–714.
9. Millipore Sigma (2020). MISSION® Lentiviral Controls, https://www.sigmaaldrich.com/US/en/technical-documents/technical-article/genomics/advanced-gene-editing/shrna-controls#trc1_trc1-5_negative_controls.
10. Ahuja, D., Sáenz-Robles, M.T., and Pipas, J.M. (2005). SV40 large T antigen targets multiple cellular pathways to elicit cellular transformation. Oncogene *24*, 7729–7745.
11. Leroy, B., Girard, L., Hollestelle, A., Minna, J.D., Gazdar, A.F., and Soussi, T. (2014). Analysis of TP53 mutation status in human cancer cell lines: a reassessment. Hum. Mutat. *35*, 756–765.
12. Engeland, K. (2018). Cell cycle arrest through indirect transcriptional repression by p53: I have a DREAM. Cell Death Differ. *25*, 114–132.
13. Georgakilas, A.G., Martin, O.A., and Bonner, W.M. (2017). p21: A Two-Faced Genome Guardian. Trends Mol. Med. *23*, 310–319.
14. Sikora, E., Mosieniak, G., and Sliwinska, M.A. (2016). Morphological and Functional Characteristic of Senescent Cancer Cells. Curr. Drug Targets *17*, 377–387.
15. Muñoz-Espín, D., and Serrano, M. (2014). Cellular senescence: from physiology to pathology. Nat. Rev. Mol. Cell Biol. *15*, 482–496.
16. Calcinotto, A., Kohli, J., Zagato, E., Pellegrini, L., Demaria, M., and Alimonti, A. (2019). Cellular Senescence: Aging, Cancer, and Injury. Physiol. Rev. *99*, 1047–1078.
17. Mc Gee, M.M. (2015). Targeting the Mitotic Catastrophe Signaling Pathway in Cancer. Mediators Inflamm. *2015*, 146282.
18. Gharbi-Ayachi, A., Labbé, J.C., Burgess, A., Vigneron, S., Strub, J.M., Brioudes, E., Van-Dorsselaer, A., Castro, A., and Lorca, T. (2010). The substrate of Greatwall kinase, Arpp19, controls mitosis by inhibiting protein phosphatase 2A. Science *330*, 1673–1677.
19. Morita, E., Colf, L.A., Karren, M.A., Sandrin, V., Rodesch, C.K., and Sundquist, W.I. (2010). Human ESCRT-III and VPS4 proteins are required for centrosome and spindle maintenance. Proc. Natl. Acad. Sci. USA *107*, 12889–12894.
20. Will, C.L., and Lührmann, R. (2011). Spliceosome structure and function. Cold Spring Harb. Perspect. Biol. *3*, a003707.
21. Rehmsmeier, M., Steffen, P., Hochsmann, M., and Giegerich, R. (2004). Fast and effective prediction of microRNA/target duplexes. RNA *10*, 1507–1517.
22. Varshavsky, A. (2019). N-degron and C-degron pathways of protein degradation. Proc. Natl. Acad. Sci. USA *116*, 358–366.
23. Prusty, A.B., Meduri, R., Prusty, B.K., Vanselow, J., Schlosser, A., and Fischer, U. (2017). Impaired spliceosomal UsnRNP assembly leads to Sm mRNA down-regulation and Sm protein degradation. J. Cell Biol. *216*, 2391–2407.
24. Housden, B.E., and Perrimon, N. (2016). Comparing CRISPR and RNAi-based screening technologies. Nat. Biotechnol. *34*, 621–623.
25. Jackson, A.L., Bartz, S.R., Schelter, J., Kobayashi, S.V., Burchard, J., Mao, M., Li, B., Cavet, G., and Linsley, P.S. (2003). Expression profiling reveals off-target gene regulation by RNAi. Nat. Biotechnol. *21*, 635–637.
26. Lin, A., Giuliano, C.J., Palladino, A., John, K.M., Abramowicz, C., Yuan, M.L., Sausville, E.L., Lukow, D.A., Liu, L., Chait, A.R., et al. (2019). Off-target toxicity is a common mechanism of action of cancer drugs undergoing clinical trials. Sci. Transl. Med. *11*, eaaw8412.
27. Lin, A., Giuliano, C.J., Sayles, N.M., and Sheltzer, J.M. (2017). CRISPR/Cas9 mutagenesis invalidates a putative cancer dependency targeted in on-going clinical trials. eLife *6*, e24179.
28. Kim, Y.K., Kim, B., and Kim, V.N. (2016). Re-evaluation of the roles of DROSHA, Export in 5, and DICER in microRNA biogenesis. Proc. Natl. Acad. Sci. USA *113*, E1881–E1889.
29. Ma, H., Zhang, J., and Wu, H. (2014). Designing Ago2-specific siRNA/shRNA to Avoid Competition with Endogenous miRNAs. Mol. Ther. Nucleic Acids *3*, e176.
30. Theile, D., Staffen, B., and Weiss, J. (2010). ATP-binding cassette transporters as pitfalls in selection of transgenic cells. Anal. Biochem. *399*, 246–250.
31. Guo, R.L., Lee, Y.T., Byrnes, C., and Miller, J.L. (2017). Puromycin Selection Confounds the RNA-Seq Profiles of Primary Human Erythroblasts. Transriptomics *5*, 1000140.
32. Akbari Moqadam, F., Pieters, R., and den Boer, M.L. (2013). The hunting of targets: challenge in miRNA research. Leukemia *27*, 16–23.
33. Bhinder, B., Shum, D., Li, M., Ibáñez, G., Vlassov, A.V., Magdaleno, S., and Djaballah, H. (2014). Discovery of a dicer-independent, cell-type dependent alternate targeting sequence generator: implications in gene silencing & pooled RNAi screens. PLoS ONE *9*, e100676.
34. Birmingham, A., Anderson, E.M., Reynolds, A., Ilsley-Tyree, D., Leake, D., Fedorov, Y., Baskerville, S., Maksimova, E., Robinson, K., Karpilow, J., et al. (2006). 3′ UTR seed matches, but not overall identity, are associated with RNAi off-targets. Nat. Methods *3*, 199–204.
35. Brennecke, J., Stark, A., Russell, R.B., and Cohen, S.M. (2005). Principles of microRNA-target recognition. PLoS Biol. *3*, e85.
36. Gu, S., Jin, L., Zhang, Y., Huang, Y., Zhang, F., Valdmanis, P.N., and Kay, M.A. (2012). The loop position of shRNAs and pre-miRNAs is critical for the accuracy of dicer processing in vivo. Cell *151*, 900–911.
37. Medley, J.C., Panzade, G., and Zinovyeva, A.Y. (2021). microRNA strand selection: Unwinding the rules. Wiley Interdiscip. Rev. RNA *12*, e1627.
38. Putzbach, W., Gao, Q.Q., Patel, M., van Dongen, S., Haluck-Kangas, A., Sarshad, A.A., Bartom, E.T., Kim, K.A., Scholtens, D.M., Hafner, M., et al. (2017). Many si/shRNAs can kill cancer cells by targeting multiple survival genes through an off-target mechanism. eLife *6*, e29702.
39. Watanabe, C., Cuellar, T.L., and Haley, B. (2016). Quantitative evaluation of first, second, and third generation hairpin systems reveals the limit of mammalian vector-based RNAi. RNA Biol. *13*, 25–33.
40. Putzbach, W., Gao, Q.Q., Patel, M., Haluck-Kangas, A., Murmann, A.E., and Peter, M.E. (2018). DISE: A Seed-Dependent RNAi Off-Target Effect That Kills Cancer Cells. Trends Cancer *4*, 10–19.
41. Gao, Q.Q., Putzbach, W.E., Murmann, A.E., Chen, S., Sarshad, A.A., Peter, J.M., Bartom, E.T., Hafner, M., and Peter, M.E. (2018). 6mer seed toxicity in tumor suppressive microRNAs. Nat. Commun. *9*, 4504.
42. Murmann, A.E., Bartom, E.T., Schipma, M.J., Vilker, J., Chen, S., and Peter, M.E. (2020). 6mer Seed Toxicity in Viral microRNAs. iScience *23*, 100737.
43. Papasaikas, P., Tejedor, J.R., Vigevani, L., and Valcárcel, J. (2015). Functional splicing network reveals extensive regulatory potential of the core spliceosomal machinery. Mol. Cell *57*, 7–22.
44. Vazquez-Arango, P., and O'Reilly, D. (2018). Variant snRNPs: New players within the spliceosome system. RNA Biol. *15*, 17–25.
45. Hofmann, J.C., Husedzinovic, A., and Gruss, O.J. (2010). The function of spliceosome components in open mitosis. Nucleus *1*, 447–459.
46. Sundaramoorthy, S., Vázquez-Novelle, M.D., Lekomtsev, S., Howell, M., and Petronczki, M. (2014). Functional genomics identifies a requirement of pre-mRNA splicing factors for sister chromatid cohesion. EMBO J. *33*, 2623–2642.
47. Weng, M.T., Lee, J.H., Wei, S.C., Li, Q., Shahamatdar, S., Hsu, D., Schetter, A.J., Swatkoski, S., Mannan, P., Garfield, S., et al. (2012). Evolutionarily conserved protein ERH controls CENP-E mRNA splicing and is required for the survival of KRAS mutant cancer cells. Proc. Natl. Acad. Sci. USA *109*, E3659–E3667.

48. Boisvert, F.-M., Ahmad, Y., Gierliński, M., Charrière, F., Lamont, D., Scott, M., Barton, G., and Lamond, A.I. (2012). A quantitative spatial proteomics analysis of proteome turnover in human cells. Mol. Cell. Proteomics *11*, M111.011429.

49. Siebring-van Olst, E., Blijlevens, M., de Menezes, R.X., van der Meulen-Muileman, I.H., Smit, E.F., and van Beusechem, V.W. (2017). A genome-wide siRNA screen for regulators of tumor suppressor p53 activity in human non-small cell lung cancer cells identifies components of the RNA splicing machinery as targets for anticancer treatment. Mol. Oncol. *11*, 534–551.

50. Blijlevens, M., Komor, M.A., Sciarrillo, R., Smit, E.F., Fijneman, R.J.A., and van Beusechem, V.W. (2020). Silencing Core Spliceosome Sm Gene Expression Induces a Cytotoxic Splicing Switch in the Proteasome Subunit Beta 3 mRNA in Non-Small Cell Lung Cancer Cells. Int. J. Mol. Sci. *21*, 4192.

51. Koedoot, E., van Steijn, E., Vermeer, M., González-Prieto, R., Vertegaal, A.C.O., Martens, J.W.M., Le Dévédec, S.E., and van de Water, B. (2021). Splicing factors control triple-negative breast cancer cell mitosis through SUN2 interaction and sororin intron retention. J. Exp. Clin. Cancer Res. *40*, 82.

52. Corbett, T.H., Griswold, D.P., Jr., Roberts, B.J., Peckham, J.C., and Schabel, F.M., Jr. (1975). Tumor induction relationships in development of transplantable cancers of the colon in mice for chemotherapy assays, with a note on carcinogen structure. Cancer Res. *35*, 2434–2439.

53. Bereta, M., Hayhurst, A., Gajda, M., Chorobik, P., Targosz, M., Marcinkiewicz, J., and Kaufman, H.L. (2007). Improving tumor targeting and therapeutic potential of Salmonella VNP20009 by displaying cell surface CEA-specific antibodies. Vaccine *25*, 4183–4192.

54. Reiss, K., Maretzky, T., Ludwig, A., Tousseyn, T., de Strooper, B., Hartmann, D., and Saftig, P. (2005). ADAM10 cleavage of N-cadherin and regulation of cell-cell adhesion and beta-catenin nuclear signalling. EMBO J. *24*, 742–752.

55. Wiederschain, D., Wee, S., Chen, L., Loo, A., Yang, G., Huang, A., Chen, Y., Caponigro, G., Yao, Y.M., Lengauer, C., et al. (2009). Single-vector inducible lentiviral RNAi system for oncology target validation. Cell Cycle *8*, 498–504.

56. Vermes, I., Haanen, C., Steffens-Nakken, H., and Reutelingsperger, C. (1995). A novel assay for apoptosis. Flow cytometric detection of phosphatidylserine expression on early apoptotic cells using fluorescein labelled Annexin V. J. Immunol. Methods *184*, 39–51.

57. Rueden, C.T., Schindelin, J., Hiner, M.C., DeZonia, B.E., Walter, A.E., Arena, E.T., and Eliceiri, K.W. (2017). ImageJ2: ImageJ for the next generation of scientific image data. BMC Bioinformatics *18*, 529.

58. Schindelin, J., Arganda-Carreras, I., Frise, E., Kaynig, V., Longair, M., Pietzsch, T., Preibisch, S., Rueden, C., Saalfeld, S., Schmid, B., et al. (2012). Fiji: an open-source platform for biological-image analysis. Nat. Methods *9*, 676–682.

59. Debacq-Chainiaux, F., Erusalimsky, J.D., Campisi, J., and Toussaint, O. (2009). Protocols to detect senescence-associated beta-galactosidase (SA-betagal) activity, a biomarker of senescent cells in culture and in vivo. Nat. Protoc. *4*, 1798–1806.

60. Raudvere, U., Kolberg, L., Kuzmin, I., Arak, T., Adler, P., Peterson, H., and Vilo, J. (2019). g:Profiler: a web server for functional enrichment analysis and conversions of gene lists (2019 update). Nucleic Acids Res. *47* (W1), W191–W198.

61. Karabasz, A., Bzowska, M., Bereta, J., Czarnek, M., Sochalska, M., and Klaus, T. (2021). Mouse IgG3 binding to macrophage-like cells is prevented by deglycosylation of the antibody or by Accutase treatment of the cells. Sci. Rep. *11*, 10295.

62. Cong, L., Ran, F.A., Cox, D., Lin, S., Barretto, R., Habib, N., Hsu, P.D., Wu, X., Jiang, W., Marraffini, L.A., and Zhang, F. (2013). Multiplex genome engineering using CRISPR/Cas systems. Science *339*, 819–823.

63. Yeo, N.C., Chavez, A., Lance-Byrne, A., Chan, Y., Menn, D., Milanova, D., Kuo, C.C., Guo, X., Sharma, S., Tung, A., et al. (2018). An enhanced CRISPR repressor for targeted mammalian gene regulation. Nat. Methods *15*, 611–616.

64. Kowarz, E., Löscher, D., and Marschalek, R. (2015). Optimized Sleeping Beauty transposons rapidly generate stable transgenic cell lines. Biotechnol. J. *10*, 647–653.

65. Mátés, L., Chuah, M.K., Belay, E., Jerchow, B., Manoj, N., Acosta-Sanchez, A., Grzela, D.P., Schmitt, A., Becker, K., Matrai, J., et al. (2009). Molecular evolution of a novel hyperactive Sleeping Beauty transposase enables robust stable gene transfer in vertebrates. Nat. Genet. *41*, 753–761.

66. Weber, K., Bartsch, U., Stocking, C., and Fehse, B. (2008). A multicolor panel of novel lentiviral "gene ontology" (LeGO) vectors for functional gene analysis. Mol. Ther. *16*, 698–706.